#2904 THE INSTITUTE OF PAPER CHEMISTRY
(Electrical Properties-Cellulose)
Project Report (1)

PROJECT REPORT FORM

Copies to: Central Records
John W. Swanson
Robert M. Leekley
R. A. Stratton
G. A. Baum (2)
Editorial Section

PROJECT NO. 2904
COOPERATOR Institute of Paper Chemist
REPORT NO. 1
DATE February 12, 1970
NOTE BOOK 2795
PAGE 1 TO 6
SIGNED Gary A. Baum
Gary A. Baum

ELECTRICAL PROPERTIES OF CELLULOSE

INTRODUCTION

It is the purpose of this first report to outline the theoretical aspects pertaining to certain electrical measurements on cellulose and to present some preliminary data taken during the first quarter. These preliminary results indicate that the technique of thermal depolarization analysis (TDA), as well as measurements of the current-voltage (I-V) characteristics, can indeed provide useful information regarding the state of the cellulosic material, viz., the nature of the conduction process, the effects of moisture content, structural alterations, and related phenomena.

THERMAL DEPOLARIZATION ANALYSIS

The ionic thermocurrent or thermal depolarization analysis (TDA) technique is a relatively new way to study the dipolar relaxation phenomena in dielectrics. Generally, dielectric relaxations in solid materials are detected by alternating current dielectric-loss measurements. This technique involves the measurement of the dielectric loss (ϵ'') over a broad frequency range and under isothermal conditions. For dipolar relaxation, a maximum in ϵ'' occurs at the resonance frequency, ω, which is inversely proportional to the relaxation time of the dipole, τ, at the measuring temperature, T $[\tau(T) = \tau_0 \exp(E/kT)]$. The characteristic parameters of the dipoles, τ_0 and E are determined by measuring τ at different temperatures.

The TDA method, however, allows the parameters τ_0 and E to be determined from a single measurement (1, 2). To illustrate this technique, consider a perfect dielectric that contains only one type of noninteracting dipoles with moment p and relaxation time, τ. In the absence of an external electric field the dipoles are randomly oriented. If one now applies an electric field, E_p, at temperature T_p, and simultaneously measures the current flow, some of the dipoles will align with the field and an exponential current decay will be observed. If the field is maintained for a length of time, $t_p \gg \tau(T_p)$, the dielectric will be polarized to saturation and the current will become constant in time. (If there are no charge carriers, either ionic or electronic, the current at saturation will be zero.) The dielectric is next cooled to a low temperature, T_0, such that $\tau(T_0)$ is very long (hours), and the external field removed. If the condenser containing the dielectric is then connected to a current detector, the electronic and atomic polarizations will relax, but the dipoles will remain oriented in the same configuration achieved at T_p. Finally, the dielectric is heated at a constant rate, $b = dT/dt$, and as $\Upsilon(T)$ gets smaller a depolarization current, $i(T)$, will be detected. This current will initially increase exponentially, reach a maximum, and then decay to zero. The functional dependence of this current may be deduced in a manner analogous to that for the case of thermoluminescence in a semiconductor.

Let P represent the electric dipole moment per unit volume in the dielectric at any instant during the warming process. The decrease in the polarization with time (temperature) during the heating process can be written:

$$dP/dt = -P/\Upsilon(T). \tag{1}$$

In this expression the minus sign represents a decrease, and $\Upsilon(T)$ is the relaxation time previously defined. Upon using the time-temperature relation $dT/dt = b$, one has

$$dP/dT = -P/b\Upsilon(T). \tag{2}$$

The variables are easily separated and integration over the limits P_o to P and T_o to T yields

$$\ln P - \ln P_o = \int_{T_o}^{T} - dT/b\Upsilon(T) \tag{3}$$

or $$P = P_o \exp\left(-\int_{T_o}^{T} dT/b\tau(T)\right). \tag{4}$$

In Equation (4), P_o represents the polarization per unit volume at temperature T_o, or more exactly, the saturation polarization resulting from the field, E_p, applied at temperature T_p. Clearly, P_o will depend on the concentration of dipoles, N, on the electric dipole moment, p, the field strength, E_p, and inversely on the polarization temperature, T_p. This dependence has been deduced by Debye (3) or Fröhlich (4) as

$$P_o = \frac{\beta N p^2 E_p}{k T_p}, \tag{5}$$

where k is Boltzmann's constant and β is a geometrical factor which depends on the possible dipolar orientation ($\beta = 1/3$ for freely rotating dipoles). Since the relaxation time at temperature T_o is assumed very long, the lower limit on the integral in Equation (4) can be replaced by zero without loss of generality.

Noting that the current density, j(T), is just equal to the velocity with which the polarization decreases, one has

$$j(T) = -dP/dt, \tag{6}$$

or combining expressions (1, 4, and 6):

$$j(T) = \left(P_o/\tau(T)\right) \exp[-\int_{o}^{T} dT/b\,\tau(T)]. \tag{7}$$

Substitutions for P_o and $\tau(T)$, $[= \tau_o \exp(E/kT)]$, then yields the functional dependence of j(T) as

$$j(T) = \frac{\beta N p^2 E_p}{\gamma_o K T_p} \exp(-E/kT) \exp\left(-\int_o^T \frac{1}{b\gamma_o} \exp(-E/kT)dT\right). \quad (8)$$

Equation (8) describes an asymmetric band and at low temperatures the exponential involving the integral is unity. Thus, at temperatures below the maximum

$$\int_o^T \frac{1}{b\gamma_o} \exp(-E/kT)dT \doteq 0 \quad (9)$$

and

$$j(T) \doteq \text{constant} \cdot \exp(-E/kT). \quad (10)$$

Equation (10), then, says that the dipole activation energy, E, can be obtained from a plot of j(T) versus $(T)^{-1}$. The temperature of the maximum, T_M, can be found by taking the derivative of Equation (8) with respect to T and setting it equal to zero. This yields

$$T_M^{\ 2} = Eb\,\gamma(T_M)/k. \quad (11)$$

Thus using Equation (10), the value of E is deduced, and from the experimentally determined value of T_M, together with b and E, γ_o can be evaluated from Equation (11).

Furthermore, it should be apparent that the area delimited by the TDA band defined by Equation (8) is proportional to the initial saturation polarization, i.e.,

$$P_o = \frac{\beta N p^2 E_p}{K T_p} = (1/b)\int_o^\infty j(T)dT. \quad (12)$$

This relationship is of importance since it allows the direct determination of the product Np^2 and consequently any changes in it due to thermal, mechanical, or chemical treatments. It should be stressed at this point that Equation (8) has been deduced for a single type of noninteracting dipole, and in this case approximation (9) and all subsequent results are deemed accurate. However, in the case of more than one type of dipole, one cannot tacitly assume that approximation (9) is valid. It can easily be seen that multiple processes (superposition of two or more TDA bands) could give significant errors in E as determined by Equation (10). Since even a small error in E can produce a large error in τ_o this point merits further consideration. Assuming that the analysis for a single TDA band is valid, the problem, then, is one of separating the overlapping bands so that Equation (8) can accurately describe each separate band.

Consider, for example, two relaxation processes which originate partially overlapping bands, A and B, having maxima at T_{MA} and T_{MB}, respectively, with $T_{MA} < T_{MB}$. These bands can be separated experimentally by the following procedure. Polarization of the dielectric at temperature T_p such that $T_{MA} < T_p < T_{MB}$, for an interval of time $t_p \doteq \tau_A(T_p) \ll \tau_B(T_p)$, will result in the dipoles of Type A polarized to saturation whereas the Type B dipoles will remain practically distributed at random. Subsequent measurements will then show a TDA band arising only from dipoles of Type A. On the other hand, the second band can be obtained by first polarizing both bands to saturation, discharging the first band (by heating to temperature T such that $T_{MA} \leq T < T_{MB}$), and then recooling to low temperatures. Upon reheating the dielectric, only the Type B band is produced. Thus, by a proper choice of polarization temperatures and times and perhaps also by successive partial discharges, it is possible to separate the total TDA band into its components. The expression for j(T) in Equation (8) can then be applied to each separate band.

IONIC CONDUCTION

It has been mentioned earlier, that after the application of an electric field to a dielectric, there may exist time-independent currents resulting from charge transport under the influence of the field. In most solids (metals, semiconductors) this conduction is electronic in origin. Many solids, however, conduct by the migration of ions in an applied field. In this case one speaks of ionic conductivity and some examples might be the alkali halide crystals and some polymers (5, 6).

It is presently believed that the ionic conductivity of solids is closely connected with lattice imperfections. For example, a perfect alkali halide crystal has a very large forbidden energy gap and is an insulator, but if this crystal is heated so that point defects of the Frenkel or Schottky-Wagner type result, the crystal can conduct by the movement of ions. In this simple scheme, one imagines the ions jumping from one defect to another. If the crystal was perfect (i.e., no defects) an ionic conductivity could be observed only if ions could leave their normal lattice sites. It is improbable that an applied field alone could produce this effect, since fields of millions of volts per centimeter would be required to dislodge an ion from its normal site. Ionic conductivity, then, must depend on thermally generated intrinsic defects or on extrinsic (foreign impurity) defects. Thus the effect of an electric field is simply to alter the statistical distribution of motion of the defect ions.

Using the ideas presented here it is possible to derive a relationship between the applied field, E, and the resultant ionic current, I. Consider, for example, the case of a Frenkel defect, such as an interstitial ion, which is generated thermally. The density of interstitial ions, n, is given by (7)

$$n = N \exp(-U_f/2kT), \tag{13}$$

where N is the concentration of ions on normal sites and U_f is the energy in eV required to generate the Frenkel defect. Since repulsive forces between ions result in potential energy barriers, an ion at an interstitial site will remain there, unless it can acquire enough energy to overcome the barrier. The probability that an ion will overcome this barrier, and move to a new interstitial site due to its thermal energy alone, is given by a Boltzmann distribution function. If ν is the vibrational frequency of the interstitial ion, the number of jumps per ion per unit time, J, is given by

$$J = \nu \exp(-U_b/kT), \tag{14}$$

where U_b is the barrier height in eV. If an external field, E, is present, however, the effective barrier heights are altered. In the direction of the applied field the barrier height is decreased by an amount $|e|Ed/2$, while antiparallel to the field the barrier height is increased by the same amount. Here $|e|$ is the ion charge and d is the distance between interstitial sites. Clearly the effect of the field is to alter the jump probabilities in the directions parallel ($\upuparrows$) and antiparallel ($\uparrow\downarrow$) to it. A net jump rate, ΔJ, may thus be defined as

$$\Delta J = J_{\upuparrows} - J_{\uparrow\downarrow}$$

or

$$\Delta J = \nu\alpha\left[\exp\left(-\frac{1}{kT}\left(U_b - \frac{|e|Ed}{2}\right)\right) - \exp\left(-\frac{1}{kT}\left(U_b + \frac{|e|Ed}{2}\right)\right)\right]$$

or

$$\Delta J = \nu\alpha \exp(-U_b/kT)\left[\exp\left(\frac{|e|Ed}{2kT}\right) - \exp\left(-\frac{|e|Ed}{2kT}\right)\right] . \qquad (15)$$

The unitless factor, α, is introduced to account for all possible jump directions. Since the difference in the square bracket defines the hyperbolic sine function, $2 \sinh \frac{|e|Ed}{2kT}$, Equation (15) can be rewritten as

$$\Delta J = \nu\alpha 2 \exp(-U_b/kT)\sinh(|e|Ed/2kT). \qquad (16)$$

The current density, j, in any system is given by

$$j = n|e|v_d , \qquad (17)$$

where v_d is a carrier drift velocity. In the present model the product $d\Delta J$ represents a drift velocity, and hence, combining Equations (13, 16 and 17):

$$j = 2\nu\alpha dN|e|\exp[(-U_b - \frac{U_f}{2})/kT] \sinh(|e|Ed/2kT) . \qquad (18)$$

Noting that $j = i/A$ and $E = V/t$ (uniform field) where i is the current, V is the applied potential, and A and t are the specimen area and thickness, respectively, one can define

$$A' = 2A\nu\alpha N|e|d \exp(-[U_b + \frac{U_f}{2}]/kT)$$

$$B' = \frac{|e|d}{2tkT} \tag{19}$$

so that

$$i = A' \sinh B'V. \tag{20}$$

Thus, this simple model predicts that in the case of ionic conductivity the current varies as the hyperbolic sine of the voltage. This dependence is in contrast to the ohmic behavior ($I \propto V$) usually observed in electronic conductors.

Equation (20) predicts an ohmic behavior only if the product $B'V \ll 1$, for then, $\sinh B'V \approx B'V$.

The resistivity, ρ, is defined as the ratio of the electric field intensity to the current density, or

$$\rho = E/J = \frac{V}{I} \cdot \frac{A}{t}. \tag{21}$$

Clearly, then, studies of the conductivity, σ ($= \frac{1}{\rho}$), as a function of temperature must be carried out at some specified voltage since in the case of ionic conductivity, I is not linear in V.

EXPERIMENTAL DETAILS

A schematic block diagram of the experimental system is shown in Figure 1. The specimen holder employs a three-electrode arrangement and its construction will be described in detail in a later report. The DPDT switch shown in Figure 1 will be fabricated at the Institute also, for reasons given shortly, and its construction will also be described in a later report.

The specimens will be in the form of thin films approximately 2.5 inches in diameter (the diameter of Electrode 1 in Figure 1). The lower main electrode (2) is 2 inches in diameter and this is the value which will determine the effective cross-sectional area used in the computations. Electrode 3 is a guard electrode that is included to prevent any surface currents which might be present, from being recorded in the current circuit.

With the switch in the up position (as shown) the Keithley 240A power supply is connected to Electrode 1 and the high impedance side of the Keithley 610CR electrometer is connected to Electrode 2. The low terminals of the power supply and electrometer, as well as the guard electrode are at ground potential. In this switch position, the resistivity, I-V characteristics and time-dependent polarization currents can be measured. When a potential is impressed upon Electrode 1, any volume current in the specimen will be detected by the electrometer. Surface currents, however, will flow to ground through the guard circuit and, hence, are not detected.

If the DPDT switch is in the down position, the power supply is taken out of the circuit, and the electrometer is connected across the specimen with the high impedance terminal to Electrode 1. In this position, TDA bands can be measured upon temperature increase.

Because cellulosic materials are expected to have a very large resistivity, especially at low temperatures and low moisture content, it is of interest to examine the capabilities of the measuring circuitry. The 240A power supply has a 0 to 1200-volt output (at 11 mA maximum) and the 610CR electrometer can detect currents smaller than 10^{-14} amps. With a typical specimen geometry factor of $A/t \doteq 10^3$ cm ($t = 1.5$ mils), and using the conservative values $V = 10^2$ volts and $I = 10^{-14}$ amps, one should be able to measure a resistivity [Equation (21)] of 10^{19} ohm-cm.

The ability to measure such a large resistivity, however, depends not only on the instrumentation but also on the ability to construct a specimen holder with very high leakage resistances. That is, any leakage path between, say, Electrodes 1 and 2 via the external circuit would give completely erroneous results. Critical areas in the sample holder and external circuit are shown as shaded circles in Figure 1. Teflon ($\rho > 10^{19}$ ohm-cm) will be used as the insulation material in the specimen holder, and in addition, all wires and BNC connectors are also insulated with Teflon. It is this requirement of high leakage resistances that dictates the special fabrication of the DPDT switch shown in Figure 1. The best commercially available switches (stock) known to the author have leakage resistances between contacts of only 10^{14} ohms (Shallcross Series 4E or Leeds and Northrup No. 33).

Additional difficulties associated with any type of high resistance measurement are AC pickup and variations in any nearby electric fields (resulting from electrostatic effects). In the present apparatus these difficulties will be overcome by the use of coaxial cable and well shielded enclosures.

Figure 1 also shows the heaters, H_1 and H_2, that will be used to vary the temperature during resistivity and TDA measurements. Heater H_1 is a 1000-ohm resistor made by wrapping 0.005-inch diameter manganin wire on a phenolic core. This heater is in contact with, but electrically insulated from, the bottom of Electrode 2. Heater H_2, not yet made, will be wrapped directly on the guard ring. These heaters are powered by a Philbrick R-100B power supply. Figure 2 shows the circuit which modifies the constant $\pm$ 300 volt dc output of the Philbrick power supply to a variable output. This circuit has been assembled. If R_1 is adjusted to $4K\Omega$, the power dissipation in the $1K\Omega$ heater (H_1) can be varied (with R_2) from zero to 2.6 watts. Assuming that the heater is 100% efficient in supplying the maximum power to Electrode 2, calculations show that the temperature of Electrode 2 (and specimen) will increase at a rate $0.12^{\circ}C/sec$. This value is the upper bound of the desired operating range.

Heaters H_1 or H_2, and an additional output H_3, are selected through Switch S_2. It is anticipated that the resistances of Heaters H_2 and H_3 will be less than $1K\Omega$, so resistors R_3 and R_4 are adjusted so that the load in any switch position is constant. In this way all power outputs are proportional to the setting of potentiometer R_2.

PRELIMINARY RESULTS

A number of measurements of resistivity, I-V characteristics, and TDA bands have been performed on some cellulose films. The material used was manufactured by the FMC Corporation, American Viscose Division, their number 124P-1, and contained 12.4% glycerine as a plasticizer, and 6.7% water at 45 R.H. The films were 1.6 mils thick and were cut into circular specimens with a diameter of approximately 2.5 inches.

The specimen holder is not yet complete, so these preliminary measurements were made using two massive electrodes of brass and thus no guard ring was included. One electrode was drilled to receive a thermometer and the whole assembly was electrically shielded. The specimen was positioned between the electrodes and the entire unit was placed on a hot plate, but electrically insulated from it. With this simple arrangement it was possible to make measurements only above room temperature. Obviously, there was no control over the ambient atmosphere and so no extensive precleaning of the specimens was performed, nor were any type of contacts made to the specimens themselves. Caution was exercised, however, in not touching specimens with the hands (to avoid oils, etc.) and the electrodes were carefully polished and cleaned to avoid irregularities and surface contamination.

Typical results of the current dependence on the applied field are shown in Figure 3. Note that both the abscissa and ordinate scales are in a dimensionless form. The values of the constants, A' and B', were deduced by a best fit plot of Equation (20) (dashed line) with the actual data. The agreement between the data and theoretical curve implies that cellulose is an ionic conductor in accordance with Equation (20).

Assuming unit charge on the ion, and with $T \approx 296^{\circ}K$ and $B' = 10^{-2}$ $volts^{-1}$, Equation (19) predicts for the jump distance, d, a value of about 200 Å. This surprisingly large value, of course, would decrease by half if the ion was divalent, etc. Mylar has also been shown to be ionic (8) according to Equation (20) and in this case the value of d at room temperature (obtained by extrapolation) is about 50 Å.

The resistivity measurements (not shown) reveal an exponential dependence on $1/T$, as expected from the model with small V, and the activation energy is calculated to be 0.93 eV. If one assumes that the room temperature carrier concentration in cellulose arises from impurities (extrinsic) rather than thermally generated defects (intrinsic), this activation energy would correspond to U_b. Thus, Equation (19) with $A' = 9 \times 10^{-11}$ amps, predicts an upper bound for the carrier concentration of about 10^{16} cm^{-3}.

TDA bands were measured on the same specimens and typical results are shown in Figures 4 and 5. In Figure 4, the uppermost band (1)is the result of a measurement on the as-received material. This sample was polarized with $Ep = 7.5 \times 10^4$ volts/cm, $Tp = 44^oC$, and $tp \doteq 2$ hours, and the subsequent heating rate was $b = 0.034^oC/sec$. Curve 1 is apparently composed of at least two subbands with maxima near 75 and 95^oC. A second run on this specimen at essentially the same polarization parameters did not reproduce Curve 1 but was about 80% less in magnitude and had no well defined maximum. These results imply that one of the bands observed in (1) is associated with the moisture content and that the initial heating releases some water, thus yielding a different curve in the second run.

The specimen was next immersed in water for one hour, in an attempt to remove some of the glycerine, and then dried for 20 hours. Using the same polarization parameters and heating rate as in (1), Curve 3 was obtained. This band also appears to contain two overlapping bands, with one maximum again near 95^oC. No effort was made to apply Equation (8) to these bands since they did not appear to result from a single relaxation process.

In an attempt to drive off additional moisture, the sample was heated for extended times at temperatures up to 100°C. After polarization at $E_p = 10^5$ volts/cm, $T_p = 125°C.$, tp = 1.5 hours, and with b = 0.037°C./sec. the curve shown in Figure 5 was obtained. Two peaks are again noted but with much smaller magnitudes (compare ordinates on Figures 4 and 5). The high temperature peak is (still) centered near 95°C. but now a well defined peak is obtained with a maximum near 47°C. At this time, it is not clear whether this lower temperature band arises from a structural phenomena that is masked in Curves 1 and 3 of Figure 4 because of some other band (i.e., moisture content) or whether it arises from structural changes caused by the extended drying process itself. Hopefully, the answer to this question and the separation of the subbands in Curves 1 and 3 will be obtained when the new sample holder is operational.

LITERATURE CITED

1. Bucci, C. and R. Fieschi., Phys. Rev. Letters 12:16(1964).

2. Bucci, C. and R. Fieschi., Phys Rev. 148:816(1966).

3. Debye, P., Polar Molecules, Chemical Catalog Co., New York, 1929.

4. Fröhlich, H., Theory of Dielectrics, Oxford University Press, London, 1958.

5. Seitz, F., The Modern Theory of Solids, McGraw Hill, New York, 1940.

6. Saito, S., Sasake, H., Nakajima, T., and Yada, K., J. of Polymer Sci., Part A-2, 6:1297(1968).

7. Kittel, C., Introduction to Solid State Physics, 2nd Edition, John Wiley and Sons, New York, 1956.

8. Amborski, L., J. of Polymer Sci. 62:330(1962).

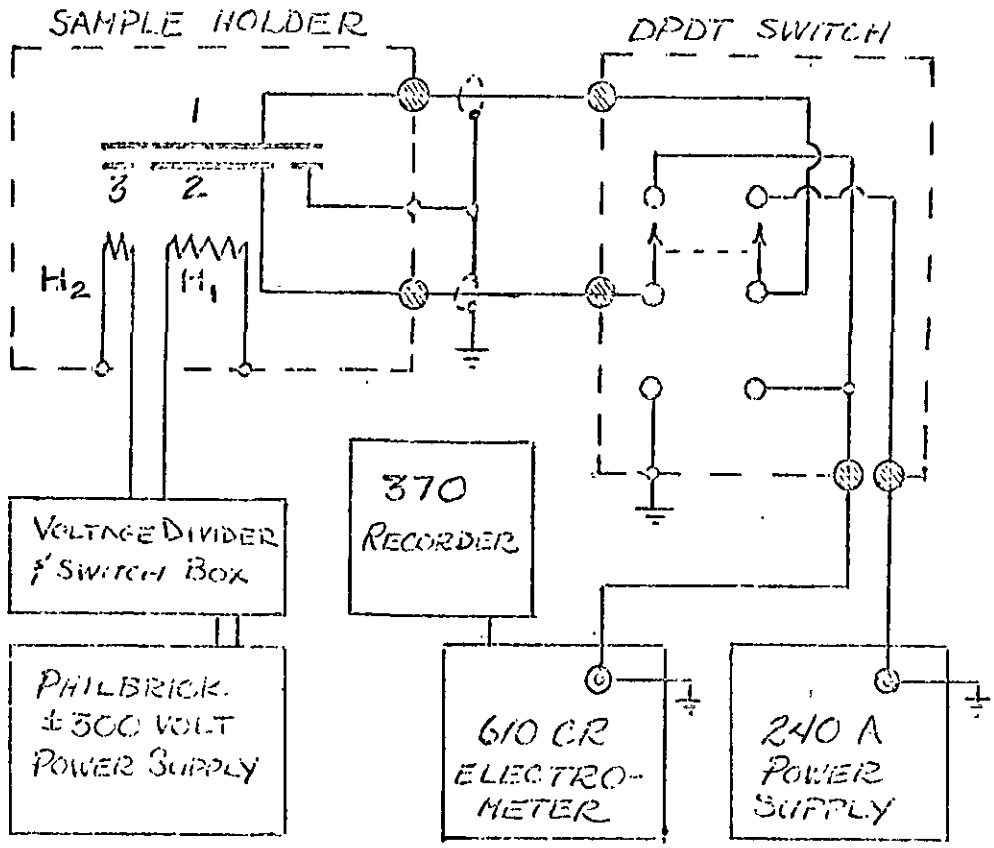

FIGURE 1: BLOCK DIAGRAM OF ELECTRICAL CIRCUITRY FOR TDA, I-V, AND ρ MEASUREMENTS. SHADED CIRCLES REPRESENT AREAS OF HIGH LEAKAGE RESISTANCE.

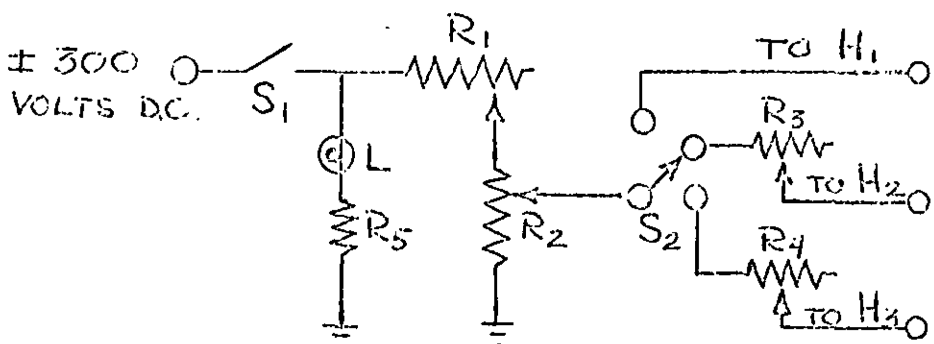

R_1	7.5 K Ω (ADJUSTABLE) - 25 WATT
R_2	5.0 K Ω (10 TURN) - 5 WATT
$R_{3,4}$	1 K Ω - 5 WATT
R_5	200 K Ω - 1/4 WATT

FIGURE 2: CIRUIT DIAGRAM OF VOLTAGE DIVIDER

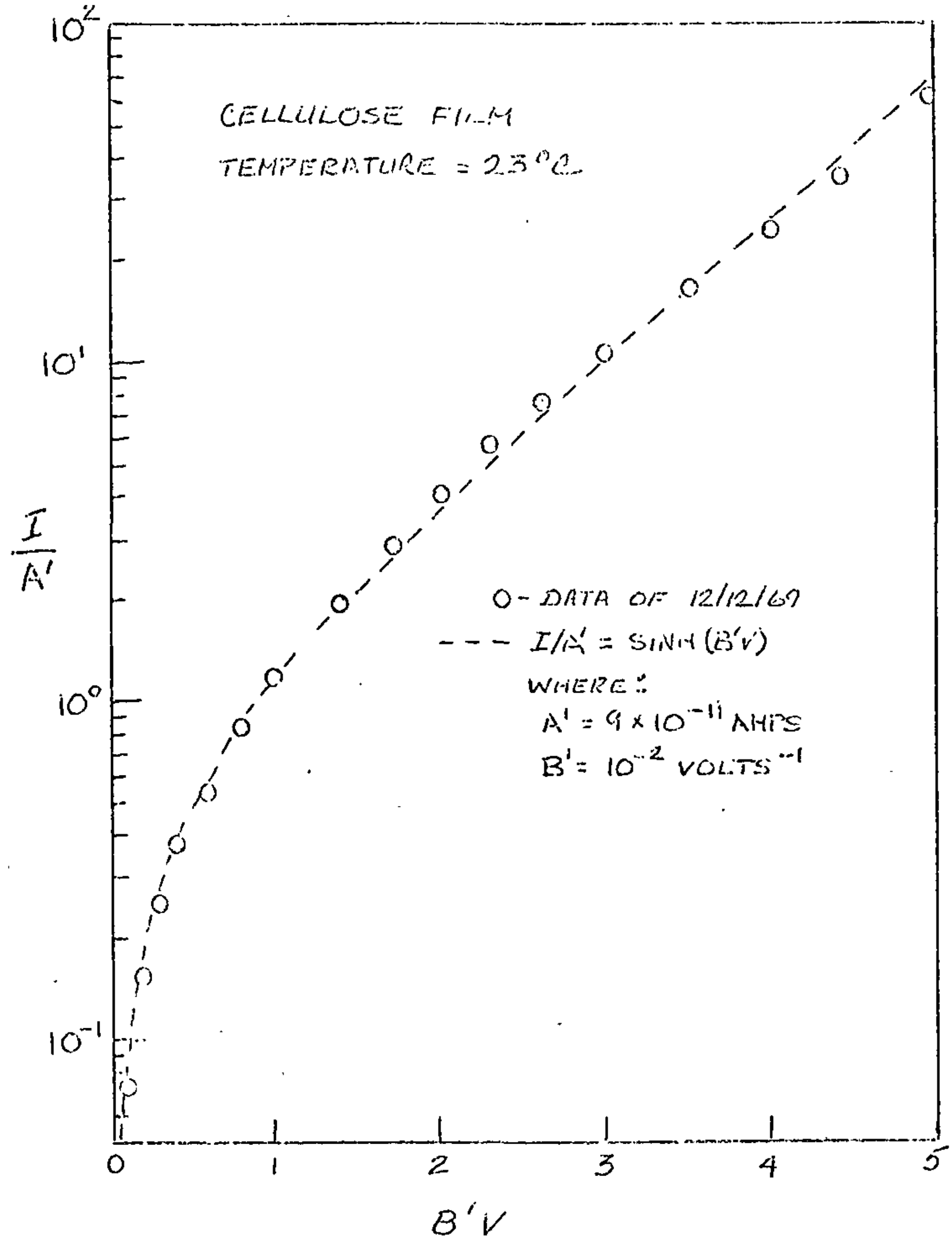

FIGURE 3: CURRENT - VOLTAGE CHARACTERISTICS

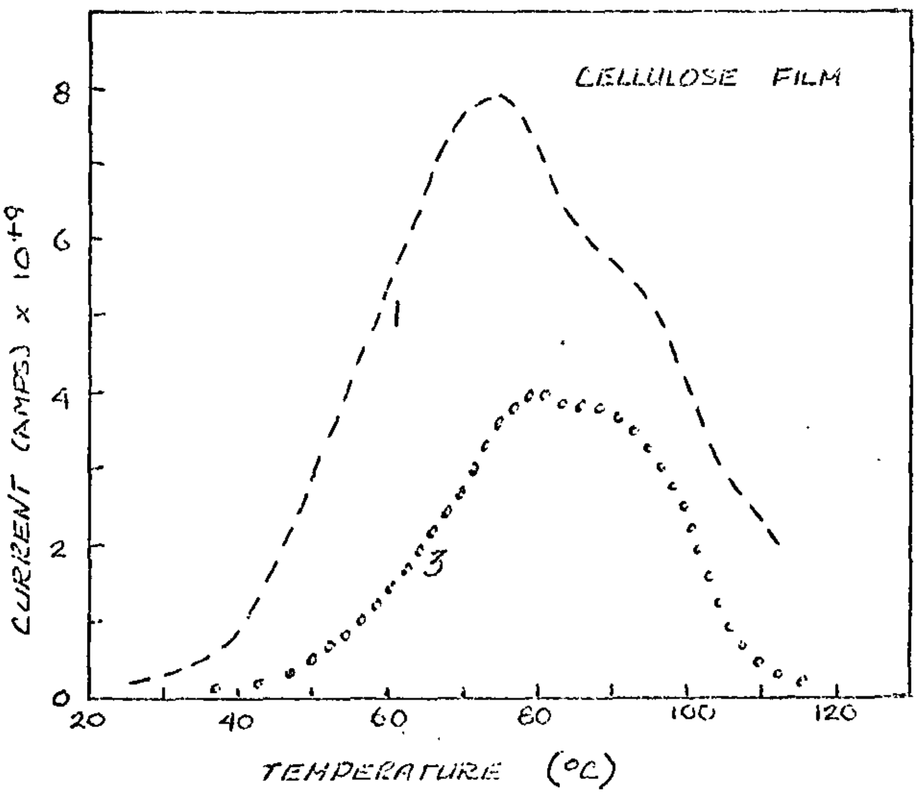

FIGURE 4: TDA BANDS - SEE TEXT

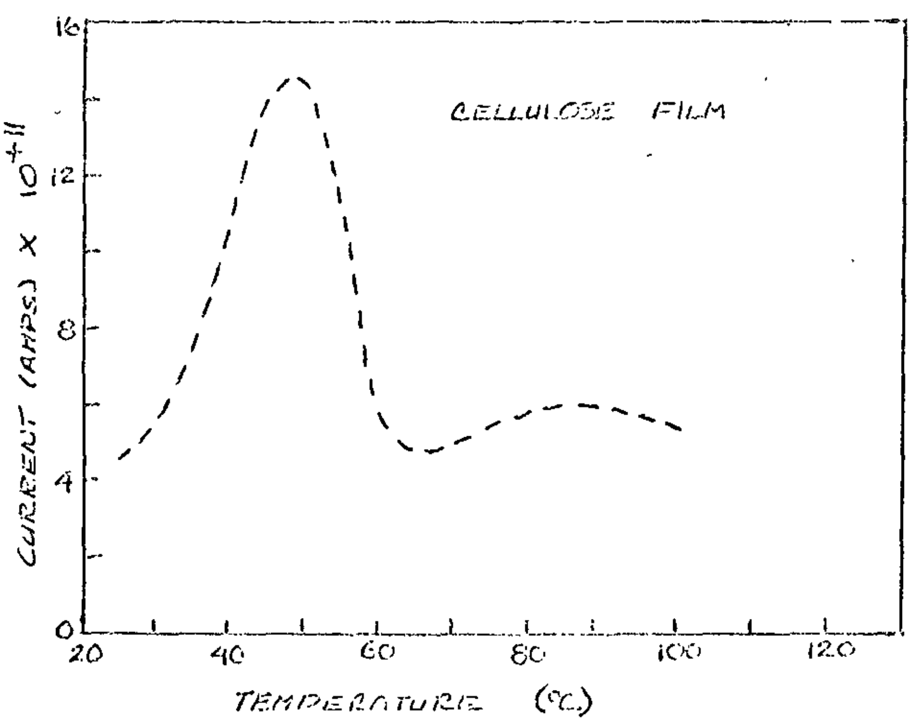

FIGURE 5: TDA BAND - SEE TEXT

PROJECT REPORT FORM

PROJECT NO. 2904
COOPERATOR IPC
REPORT NO. 2
DATE September 22, 1970
NOTE BOOK 2795
PAGE 7 TO 22
SIGNED G. A. Baum

G. A. Baum

Copies to: Central Records
John W. Swanson
Robert M. Leekley
R. A. Stratton
G. A. Baum (2)
Mr. Weiner

ELECTRICAL PROPERTIES OF CELLULOSE

INTRODUCTION

Since the last report, work on this project can be divided into three areas. The first of these deals with the effect of moisture content on the conductivity of cellulosic materials. A review of the data presented in the literature reveals that these experimental results may be more meaningful if log conductivity is examined as a function of inverse moisture content. The conductivity is then represented by the sum of two Boltzmann-type terms in M^{-1}. When plotted in this fashion the mobility of the charge carriers, rather than the creation of carriers, seems to be the conductivity-controlling factor, at least for $M > 3\%$. The M^{-1} dependence is assumed to arise because of the effect of moisture on the dielectric constant of the cellulosic material. These ideas are still under investigation.

The second area, discussed in detail in the next section, deals with some experimental studies of thermal depolarization currents in Du Pont Type A Mylar film. A recent article on the same topic prompted this investigation (1). Agreement between the two investigations is good, although the authors of the article failed to distinguish an additional low-temperature peak and have seemingly misused the theoretical expressions given by Bucci et al. (2). This paper, to my knowledge, is the first to appear since the original work of Bucci et al. in 1966. Within the last several months, two additional papers have been published on this technique, by a group in Germany (3, 4). (Surprisingly, no reference is made to the work of Bucci *et al.*) One of these papers derives the basic equations pertinent to the theory. Although in a slightly different form, these derivations are similar to those presented by me in Project Report 1, pages 2 through 7. The third area, also discussed in a later section, deals with thermal depolarization current measurements on cellulosic film at low temperatures (to -50°C.).

THERMAL DEPOLARIZATION CURRENTS IN MYLAR

EXPERIMENTAL RESULTS

Lilly, Stewart, and Henderson (LSH) (1) have recently studied thermally stimulated currents in Mylar (polyethylene terephthalate). Their measurements were made on Type A material, 5 mils thick, using polarizing fields up to 240 kv./cm. and heating rates of about 0.1°K/sec. In general, their results indicate a broad band centered near 400°K. These authors conclude that the Bucci *et al.* (2) theory does not fit the Mylar data. A close examination of their results, however, leads one to suspect that their treatment of the data is in error. For this reason, and because Mylar is readily available, it appeared worthwhile to make some measurements on this material. It was felt that this would provide valuable experience as well as affording comparisons with the published results.

Measurements were made on 1-mil, Type A Du Pont Mylar at polarizing field strengths, E_p , up to 200 kv./cm. In an attempt to reproduce the LSH results, the polarization temperature, T_p , was selected as 140°C. and the heating rate, b , as 0.1°K/sec. (after LSH). All measurements were made in air using the specimen holder described in Project Report 1 (PR 1) (5).

Figure 1 displays the thermal depolarization current results as a function of temperature. A well-defined maximum occurs in the temperature range 396 to 398°K,

Figure 1

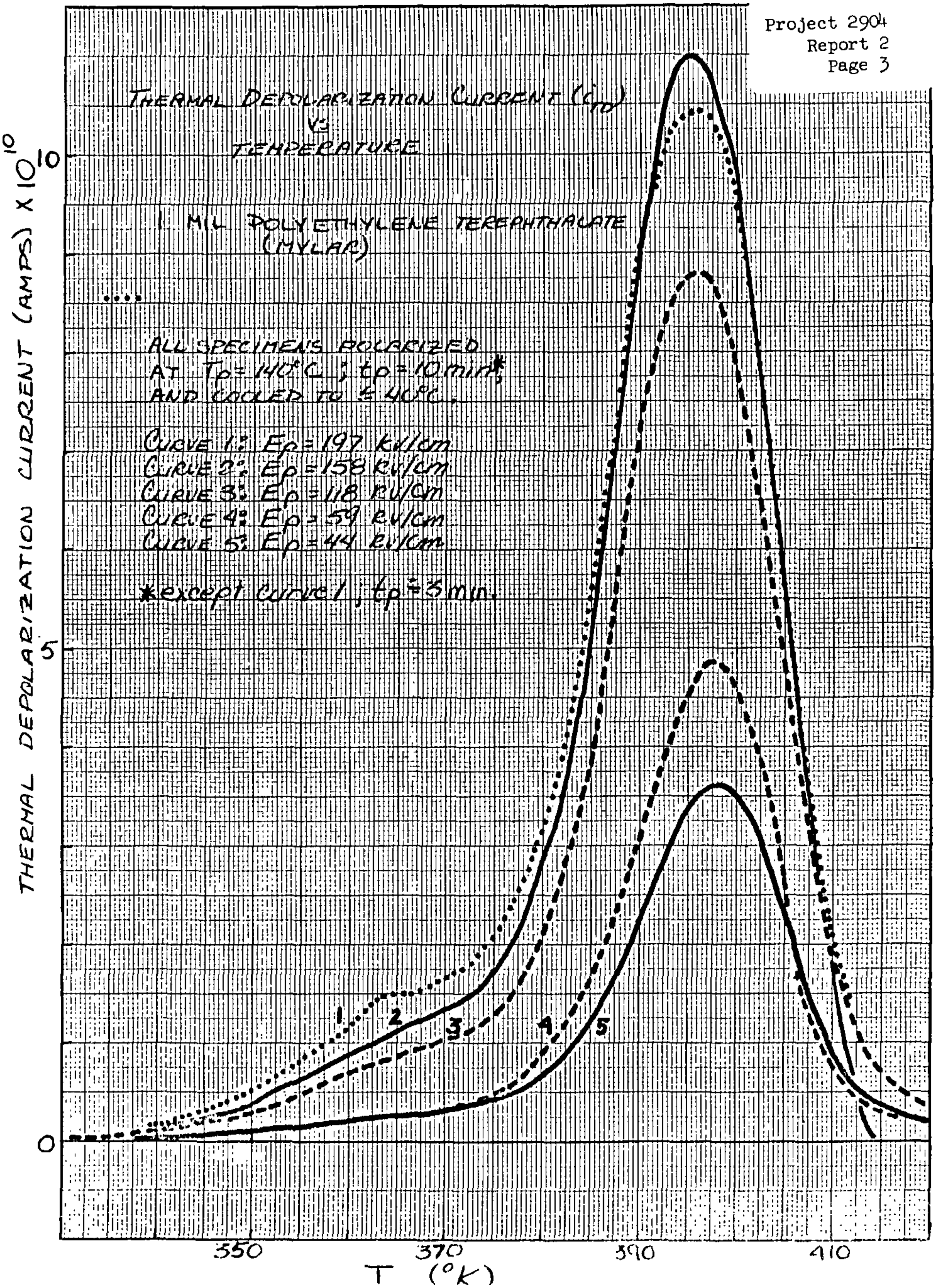
THERMAL DEPOLARIZATION CURRENT (i_D) VS TEMPERATURE
1 MIL POLYETHYLENE TEREPHTHALATE (MYLAR)
ALL SPECIMENS POLARIZED AT T_p = 140°C ; t_p = 10 min* AND COOLED TO ≤ 40°C.
Curve 1: E_p = 197 kV/cm
Curve 2: E_p = 158 kV/cm
Curve 3: E_p = 118 kV/cm
Curve 4: E_p = 59 kV/cm
Curve 5: E_p = 44 kV/cm
*except Curve 1, t_p = 5 min.
THERMAL DEPOLARIZATION CURRENT (AMPS) X 10^{10}
10
5
0
1
2
3
4
5
350
370
390
410
T (°K)

with a half width of about 20°K. This is in contrast to the broader peaks reported by LSH with half widths around 35°K. The temperature of the maximum in the LSH results ranged from 385 to 425°K with an average near 400°K.

Figure 1 also suggests that another peak may be present at lower temperatures, near 360 to 370°K. This is more obvious in Fig. 2 which depicts $\ln i_{TD}$ as a function of $10^3/T$. Two distinct exponential regions are apparent. In the high-temperature region, the calculated activation energies [see Equation (10), PR1] range from 1.52 to 1.63 eV, while in the low-temperature region E is around 0.9 eV. One would expect the low-temperature slope, however, to be affected by the "tail" of the high-temperature peak, so this latter value must be examined with caution.

Since E and Tm (temperature of the maximum) and the parameters T_p and t_p are very nearly the same for all the high-temperature curves, Equation (8), PR1, predicts that the maximum thermal depolarization current, $i_{TD}(max)$, should be linear with E_p if the peak is of dipolar origin. A plot of $i_{TD}(max)$ versus E_p (not shown) illustrates that this is the case for low E_p, but that above approximately 150 kv./cm. deviations from linearity occur. This may imply that the peak near 397°K in Mylar does not result from dipole reorientations.

In an attempt to verify the existence of the low-temperature peak, the specimen was polarized at lower temperatures at a number of field strengths and these results are shown in Fig. 3. With $T_p \cong 85$°C., curves 1, 2, and 3 are obtained and the effect of decreasing field strength on the relative magnitudes of the high- and low-temperature peaks can be observed. Note once again that the high-temperature peak, now greatly diminished, still has a maximum in the range 394 to 400°K. According to the equations given in PR1, T_m should be independent

Figure 2

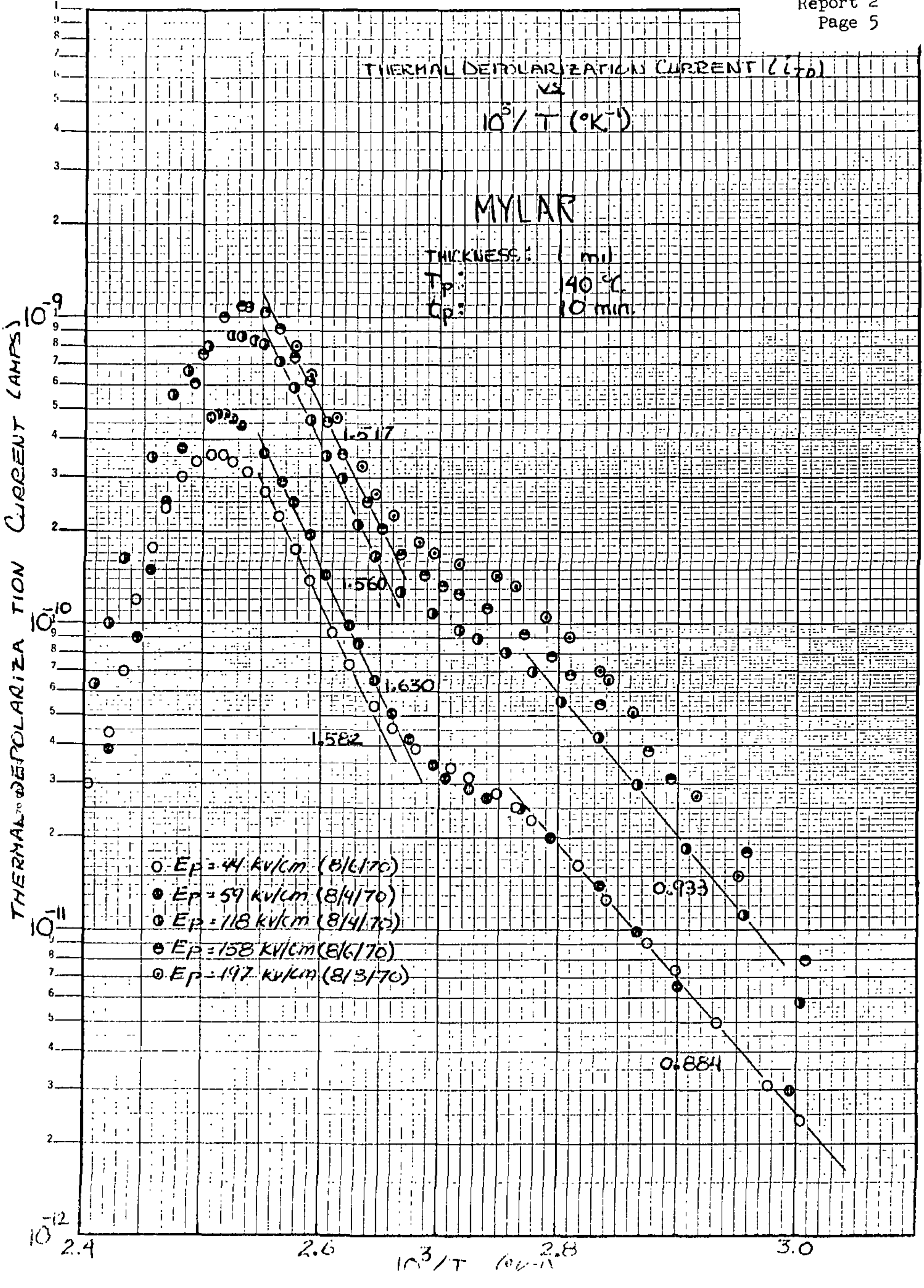
THERMAL DEPOLARIZATION CURRENT (i_{TD}) vs $10^3/T$ (°K^{-1})
MYLAR
THICKNESS: 1 mil
T_p: 140 °C
t_p: 10 min.
1.517
1.560
1.630
1.582
0.933
0.884
○ Ep = 44 kv/cm (8/6/70)
● Ep = 59 kv/cm (8/4/70)
Ep = 118 kv/cm (8/4/70)
Ep = 158 kv/cm (8/6/70)
Ep = 197 kv/cm (8/3/70)
THERMAL DEPOLARIZATION CURRENT (AMPS)
$10^3/T$ (°K^{-1})
2.4
2.6
2.8
3.0
10^{-9}
10^{-10}
10^{-11}
10^{-12}

Figure 3

Project 2904
Report 2
Page 6

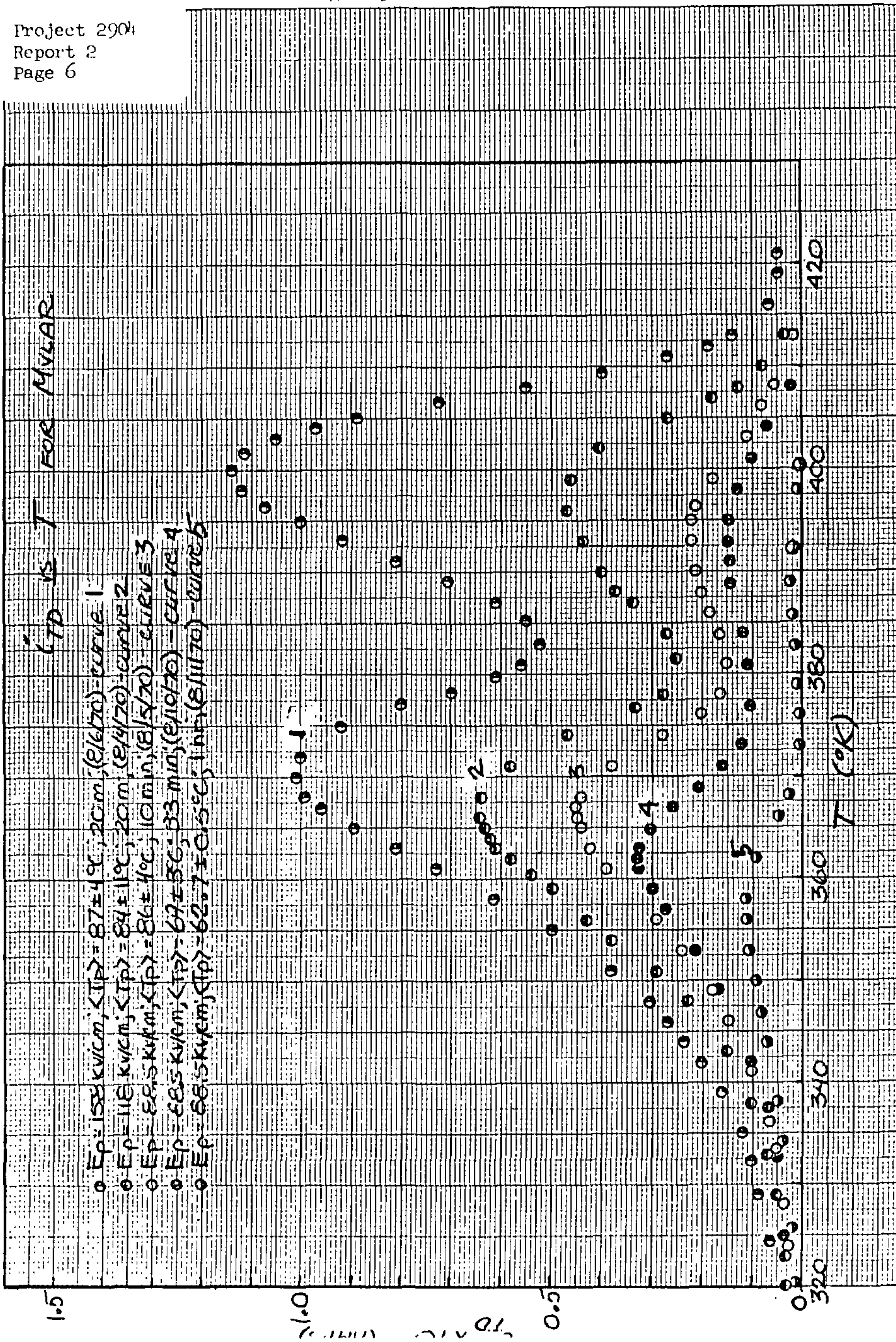

of both E_p and T_p . This appears to be the case for the high-temperature peak, thus lending support to the applicability of this theory to Mylar.

Also of significance in Fig. 3 is the verification of a low-temperature peak with a maximum near 365°K. Note that the temperature of the maximum shifts slightly to lower temperatures as the magnitude of the high-temperature maximum decreases. This probably indicates that the high-temperature peak is still important, at least down to 360°K, and that $i_{TD}(max)$ for the low-temperature peak is still a superposition of components of both peaks. An alternative explanation for the shift to lower temperatures is that the temperature maximum is dependent upon the polarization temperature, that is, the peak is not of dipolar origin. A plot of $\ln i_{TD}$ versus T^{-1} , however, does yield a straight line on the low-temperature side of the peak, as shown in Fig. 4. This suggests that the origin of this band <u>is</u> dipolar in nature, in accordance with Equation (8), PR1.

The activation energies calculated from the curves in Fig. 4 range from 0.73 to 0.77 eV . These values are lower than those found for the low-temperature peaks from Fig. 2, thus indicating how errors might arise if attempts are not made to separate overlapping bands. In fact, since the overlapping portions of the peaks shown in Fig. 3 are not certain, the E values determined from Fig. 4 may still be slightly large. There does not seem to be any correlation between the variation of E and the magnitude of the high-temperature band, however, and thus errors arising from "overlap" at the lower temperatures are assumed minimal.

Also of interest on Fig. 3 are the differences between curves 3, 4, and 5. Note that E_p is the same for these curves, but that T_p has values of 86, 69, and 63°C., respectively. The respective relaxation times at these temperatures are about 6, 23, and 40 minutes and hence the polarization times, t_p , given on

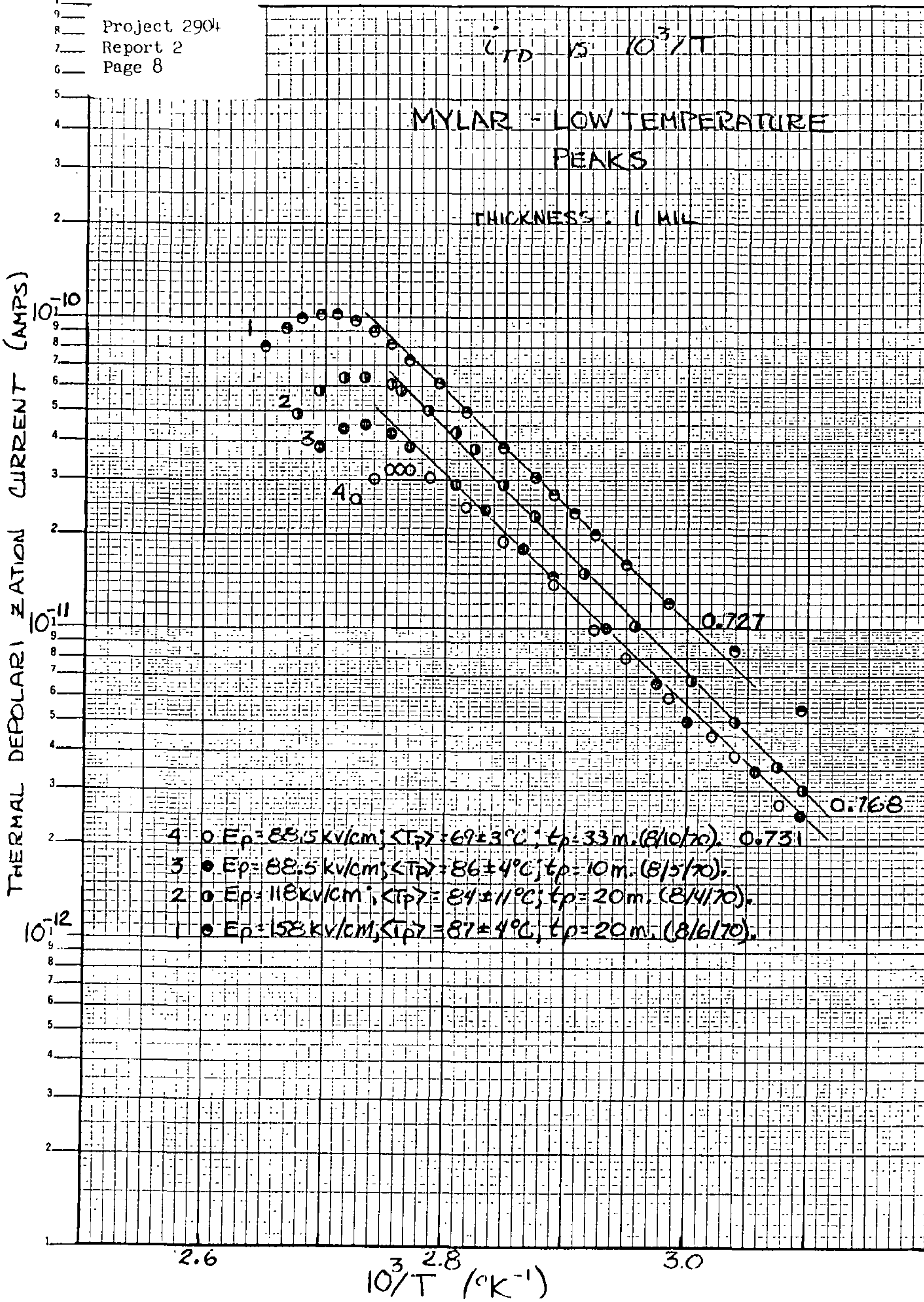
i_{TD} vs $10^3/T$
MYLAR - LOW TEMPERATURE PEAKS
THICKNESS : 1 MIL
THERMAL DEPOLARIZATION CURRENT (AMPS)
10^{-10}
10^{-11}
10^{-12}
0.727
0.768
0.731
4 o Ep=88.5 kv/cm; <Tp>=69±3°C; tp=33 m. (8/10/70).
3 ● Ep=88.5 kv/cm; <Tp>=86±4°C; tp=10 m. (8/5/70).
2 o Ep=118 kv/cm; <Tp>=84±11°C; tp=20 m. (8/4/70).
1 ● Ep=158 kv/cm; <Tp>=87±4°C; tp=20 m. (8/6/70).
2.6
2.8
3.0
$10^3/T$ (°K^{-1})

Fig. 3 are roughly 1.5 time constants. [The relaxation times are computed using Equation (11), PR1, with $E = 0.74eV$ and $\tau_0 = 10^{-8}$ sec.] The equations relating polarization and current with time are developed in Appendix I.

It would appear, then, that the difference in magnitude between curves 3, 4, and 5 on Fig. 3 cannot arise solely because of differences in relaxation times, but from some other effect. One possibility might be the glass transition in poly(ethylene terephthalate). The glass transition in amorphous Mylar is near 68°C., whereas for semicrystalline material it varies up to about 80°C. (6). The crystallinity of the Mylar used in this study is not known, but if it is assumed that T_g lies within the stated range, then, since T_p (curve 3) > T_g and T_p (curve 5) < T_g, the low-temperature band may be associated with the glass transition. This is a weak argument, however, because the activation energy involved (~0.7eV) is much smaller than that usually associated with the glass transition in Mylar (6, 7).

The effect of the glass on the high-temperature band is uncertain because in this case the decreasing magnitude can be accounted for by only the increase in relaxation times at the lower polarization temperatures. This is because the relaxation times for this band are considerably longer than in the low-temperature band, e.g, 5.6 hours at 86°C., and thus $t_p \ll \tau(T_p)$.

Figure 5 shows the relaxation time as a function of inverse temperature. The two solid lines represent τ for the low- and high-temperature bands. These were obtained using Equations (10) and (11), PR1, and using average values of E and T_m. In the original paper of Bucci et al. (2), it is pointed out that the relaxation time can be related to the whole $i(T)$ curve by

$$\tau(T) = \left[\int_{t(T)}^{\infty} i(t)dt\right]/i(T) \qquad (1)$$

Figure 5

Project 2904
Report 2
Page 10

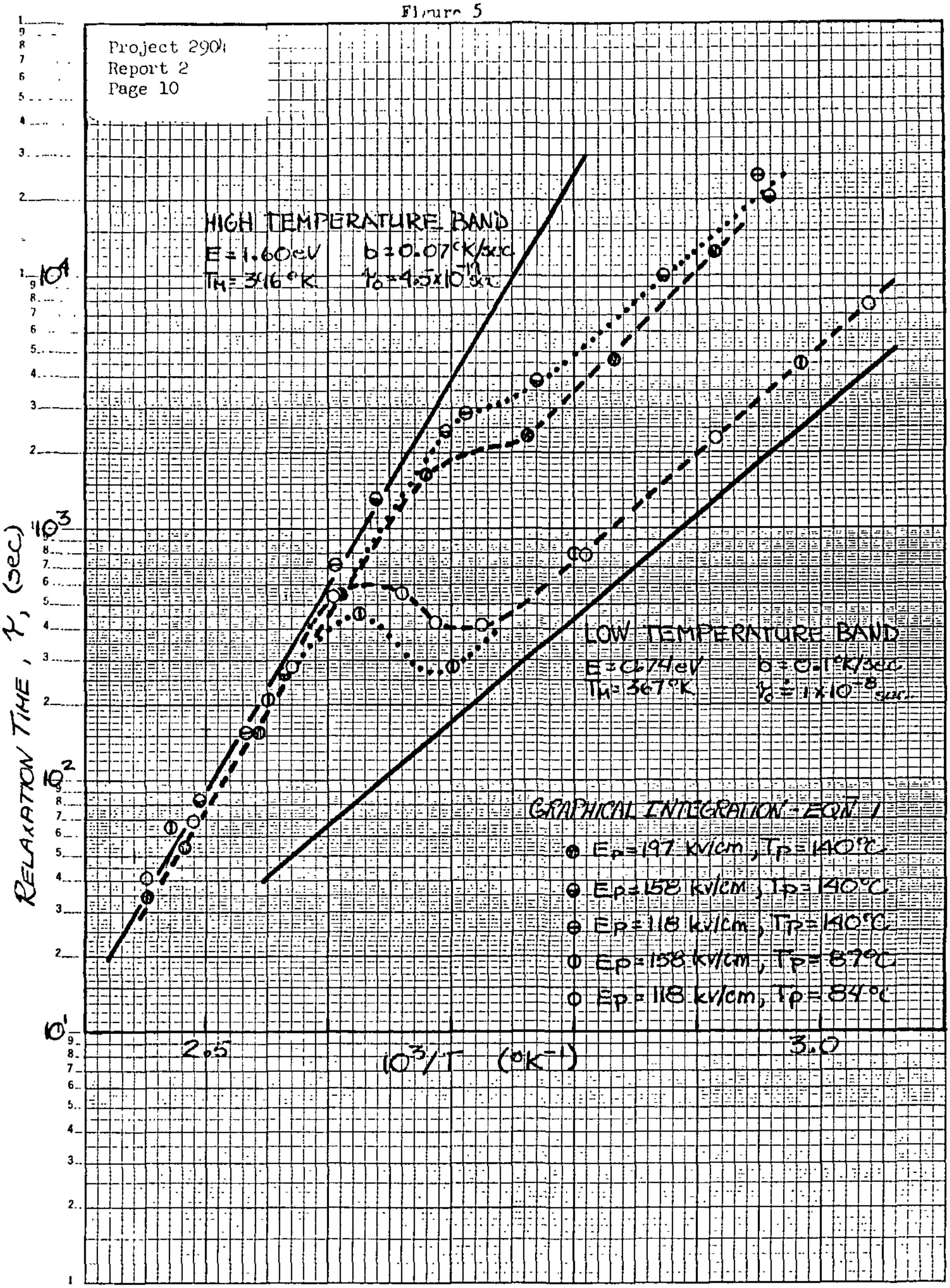

where t is time and T is temperature. The advantage to this approach is that the heating rate, b, is not involved, since the form of the original data is a current *versus* time plot. This expression can be integrated graphically. This has been done for a number of specimens and the results are plotted in Fig. 5.

For the high-temperature band, the agreement between the relaxation times, as computed by the two techniques, is good, as would be expected. This is in contrast, however, to the work of LSH who reported differences of orders of magnitude between the two techniques.

Equation (1) applies only to a single thermal depolarization band and thus the graphical integration of the data here, which contains two bands, results in a composite of the separate relaxation times. Thus the S-shaped character of the data-point curves in Fig. 5 is strictly a mathematical artifact. If the two depolarization bands were closer together in temperature, a smooth transition of relaxation times would be expected, whereas for completely separated bands, Equation (1) would apply to each individually. This also explains the fact that the low-temperature-band data points all lie above the relaxation time obtained by the first method (solid line). That is, at the lower temperatures, the current-time integral (charge) for the high-temperature band is always present and thus represents an additive factor. This slightly affects the slope of the relaxation time for the low-temperature band and also displaces it upwards. If the shape of the high-temperature band is estimated and subtracted before the graphical integration, the resultant relaxation times for the lower band fall in the vicinity of the solid line.

In PR1, two techniques were described whereby two superimposed peaks could be separated. One of these techniques involved polarization at temperatures low enough to prohibit one of the peaks from being completely polarized. This is the procedure used in obtaining Fig. 3. Thus, if the low-temperature peak of, say, curve 2 on Fig. 4 (E_p = 118 kv./cm.) was subtracted from the E_p = 118 kv./cm. curve (◑) on Fig. 2, one would expect to see the "pure" high-temperature band. This is shown in Fig. 6, and the agreement between the difference points (open circles) and the extended slope (E = 1.56 eV) is fairly good.

The second technique of peak separation, that of a partial depolarization, was also attempted and yielded equally successful results. In this case, however, the data points at the lowest temperatures consistently fell below the projected slope, indicating that a portion of the high-temperature peak had apparently depolarized along with the low-temperature band.

In order to compare the theory presented in PR1 with the experimental results on the high-temperature side of the maximum, a theoretical curve of i(T) was computed and is also shown on Fig. 6. This curve was calculated using Equation (8), PR1, with parameters: $b = 0.07^{o}K/sec.$, E = 1.6 eV, and $\tau_0 = 7 \times 10^{-19}$ sec. In an abbreviated form, Equation (8) can be written:

$$i(T) = C \exp(-E/kT) \exp(-u) \qquad (2)$$

where C is a constant, and

$$u = \int_0^T (1/b\tau_0) \exp(-E/kT)dT \qquad (3).$$

The integral u can be integrated by parts and developed into a convergent series (8), i.e.,

Figure 6

Project 2904
Report 2
Page 13

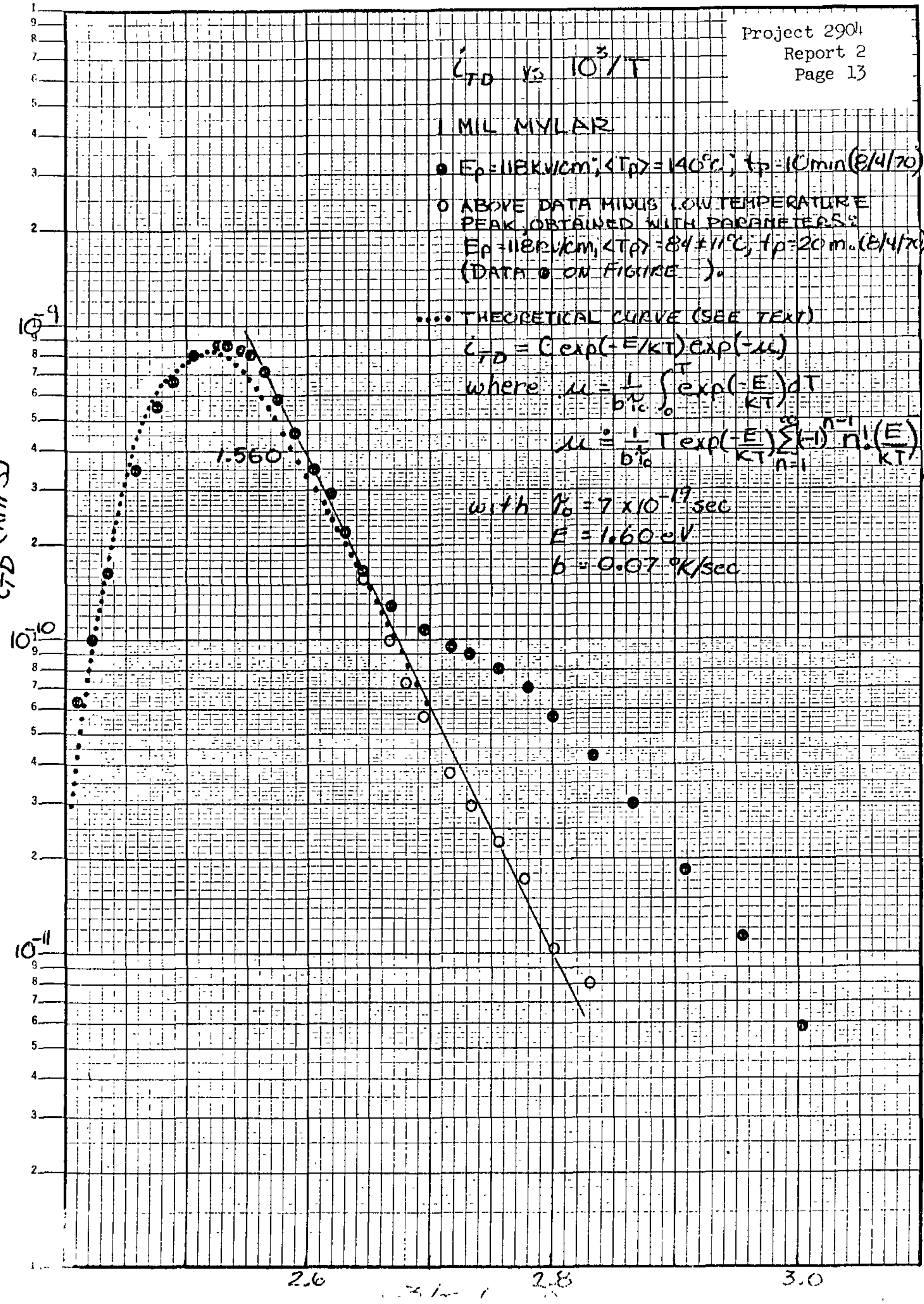

$$u = (1/b\tau_0)[T\exp(-E/kT) - (E/k)\int_0^T \exp(-E/kT)T^{-1}dT] \ ,$$

$$u = (b\tau_0)^{-1}T\exp(-E/kT)\sum_{n=1}^{\infty}(-1)^{n-1}n!(E/kT)^{-n} \qquad (4) \ .$$

In the calculation made here, the series was truncated after the first two terms. This resulted in about a 1% error in u. The pre-exponential factor, C, was determined by fitting the theoretical curve on the low-temperature side of the maximum, where $u = 0$. The agreement between theory and the experimental points on the high-temperature side of the maximum is quite good, supporting the orientation polarization picture for Mylar.

In an attempt to locate the glass transition temperature, the dc resistance of the Mylar was measured as a function of temperature. These results are shown in Fig. 7, and the change in slope of $\ln R$ versus T^{-1} occurs in the vicinity of 80°C. This is assumed to be the glass transition temperature. There are two other features of interest on Fig. 7. The first of these is the magnitude of the resistance at temperatures above T_g. At 400°K ($10^3/T = 2.5$), the resistance of the specimen is around 10^{10} ohms, and this value is significant because the value of the external resistor used in the measuring circuit is also 10^{10} ohms. Thus at this temperature the external resistance in the circuit is also effectively controlling the current and introducing a 100% error into the magnitude of the current. At higher temperatures the error is even greater, while the error decreases at lower temperatures (1% error at 370°K). Thus in the preceding figures the current magnitudes for the high-temperature band are in error. This has been confirmed by using a 10^7-ohm resistor. The previous discussions are not affected by this error except that the slope of the high-temperature band increases to 1.66 eV, and, of course, the magnitudes of the high-temperature

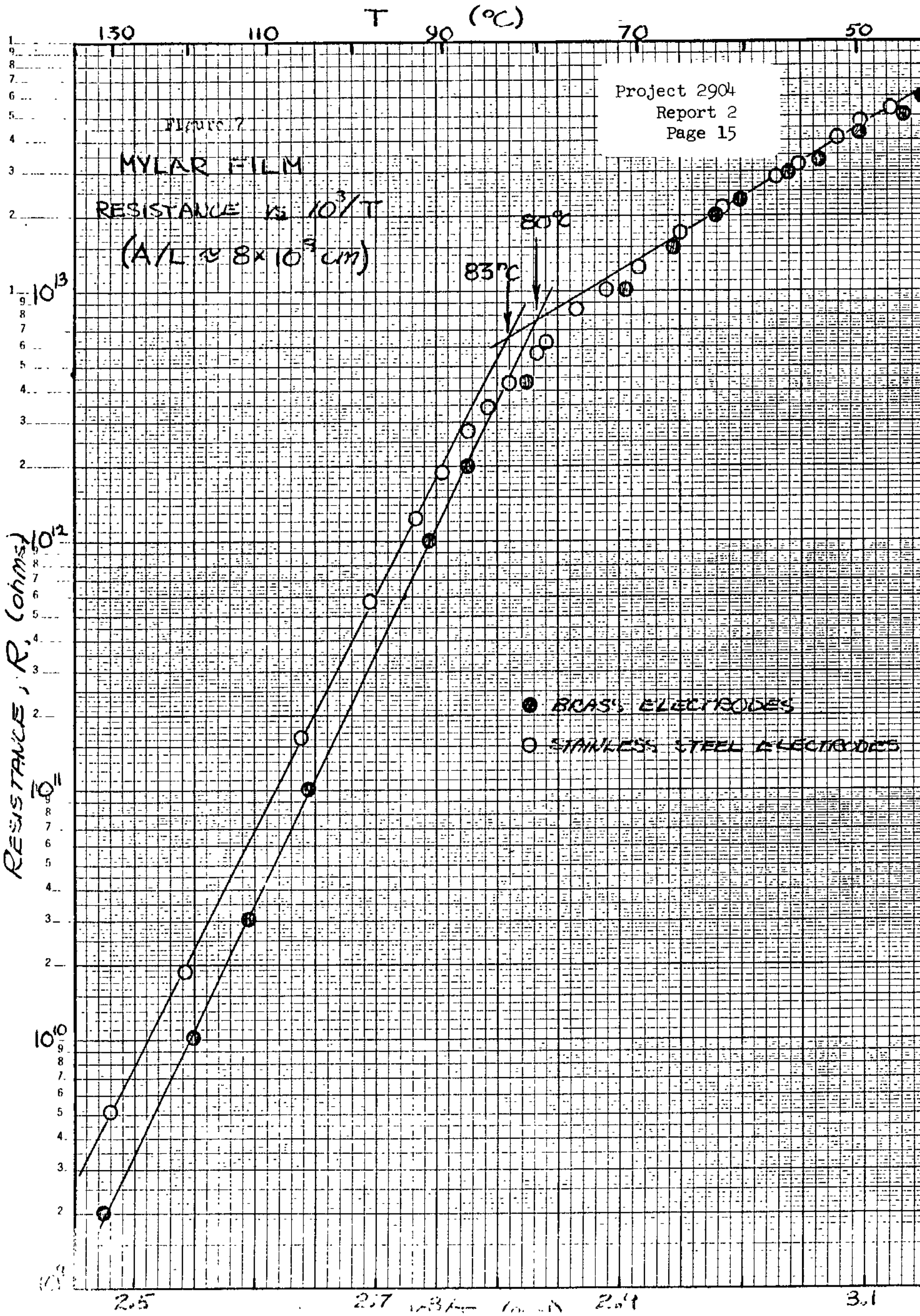
Figure 7
MYLAR FILM
RESISTANCE vs $10^3/T$
($A/L \approx 8 \times 10^3$ cm)
T (°C)
130
110
90
70
50
80°C
83°C
BRASS ELECTRODES
STAINLESS STEEL ELECTRODES
RESISTANCE, R, (ohms)
10^{13}
10^{12}
10^{11}
10^{10}
2.5
2.7
2.9
3.1

band are off by a factor of about 2 at the maximum. The theoretical curve in Fig. 6 as well as the relaxation times for the high-temperature band in Fig. 5 are slightly altered by making the necessary corrections, but not enough to warrant replotting these data. Since it was necessary to generate the correction equations for $i_{TD}(T)$ and $\tau(T)$ in order to make these statements, these are included in Appendix II for future reference.

The second feature of interest in Fig. 7 is the difference in the measured resistance at temperatures above the glass transition, when using different electrode materials. This may indicate that surface effects (interfacial polarization) are present, and this would have a bearing on the thermal depolarization results also.

DISCUSSION OF MYLAR RESULTS

From the scatter in their results, LSH were inconclusive as to whether the effect observed by them was dipolar in origin. The evidence presented in the preceding section, however, suggests that the thermal depolarization theory fits the Mylar data quite well. The problem, then, is to elucidate the dipoles or dipole groups responsible for the observed peaks.

There is a fundamental difference between the τ_0 values calculated for the two bands. Normally, τ_0 would be expected to be of the order of the inverse vibrational frequency, ν^{-1}, of an atom at temperature T, i.e., $\nu^{-1} \cong h/kT \cong 10^{-13}$ sec. For the low-temperature process reported here, τ_0 is considerably larger than this value, viz., 10^{-8} sec., while for the high-temperature band, $\tau_0 \cong 10^{-18}$ sec. The polarization process is an order-disorder process, however, and thus entropy effects must be accounted for in τ_0. From chemical rate theory it follows [e.g., see Reference (3)],

$$\tau_0 = [ah/kT] \exp(-S/k) ,$$

where S is the entropy of activation and a is a sterical factor pertaining to dipole rotations. It is obvious from this expression that $S > 0$ for the high-temperature process reported here, but $S < 0$ for the low-temperature band. In terms of the initial polarization, this means that for the low-temperature process the application of a field E_p , at constant temperature T_p , resulted in an increase in the molecular disorder (entropy). This is understandable if one assumes that in the absence of a field the dipoles are in a well-ordered state such as might be expected in a crystalline solid. The field can thus only decrease the existing order by turning some of the dipoles into different directions. Subsequent heating to the final or activated state (with $E_p = 0$) then returns the system to a higher ordered state and $S < 0$. For the high-temperature process, on the other hand, the reverse is true. The positive S implies that dipoles were aligned with the field during the polarization process, and that randomness was restored upon reheating.

These differences between the characteristic relaxation times make it very tempting to assign the low-temperature process to the crystalline regions of the Mylar, and the high-temperature process to the amorphous regions. This interpretation, however, is not consistent with the data of Fig. 3 which suggested that the low-temperature process might be influenced by the glass transition. The activation energy (~0.7 eV) for the low-temperature process would suggest that the dipoles are relatively unhindered, while the higher activation energy for the high-temperature process indicates a more restrictive environment for this process.

Reddish (7) studied the dielectric properties of poly(ethylene terephthalate) and found three ac dielectric processes. The low-temperature process (near -40°C. at 100 Hz) he attributed to the presence of -OH groups. At very high temperatures the observed process was assumed to result from charge conduction. The third process (centered near 105°C. at 100 Hz) was attributed to relaxations involving the main polymer chain (alpha relaxation process). For this latter process Reddish reported $\tau_0 = 10^{-64}$ sec. and $E = 3.9$ eV . These values differ considerably from those found in this work, and from this standpoint, correlations between the two types of measurements are difficult.

The activation energy calculated for the conduction process from Fig. 7 is about 1.85 eV , at temperatures above the glass transition. This same value was also reported by Amborski (9) and Reddish (7). Interestingly enough, this is close to the activation energy reported for the high-temperature activation process. This would suggest that this process is related to a space charge or interfacial polarization. Nedetzka et al. (3) discuss such mechanisms and conclude that they should display a depolarization curve similar to that of a true orientational polarization. McDonald (10) first described the buildup of space charges, resulting from blocking electrodes, and if this effect is responsible for the high-temperature process reported here, peak heights and widths will be altered by using different electrode materials. It is anticipated that this can be done in the near future to clarify the nature of the high-temperature peak.

In summary, both bands can be described by the thermal depolarization current theory. The low-temperature band has a maximum near the glass transition temperature, but the small activation energy precludes a correlation with the alpha-process observed by others using ac techniques. Entropy considerations imply that this effect originates in highly ordered regions of the material, where the effect of an external electric field is to create disorder. The second band has a maximum about 45 degrees above the glass transition temperature and, although the TDC theory fits this process, it is suspected that this band originates from a space charge or interfacial polarization effect.

CELLULOSE FILM RESULTS

The guarded electrode specimen holder, referred to in PR1, is depicted in Fig. 8. This figure is nearly to scale, and the upper portion of the specimen holder, called the vacuum feedthru assembly, has been rotated 90° for clarity. To provide high leakage resistances, the electrode leads are insulated by Teflon and glass sleeves through the vacuum feedthru. Vacuum seals are made with Varian Torr Seal Epoxy. In order to avoid thermal emf's in the thermocouple leads that might be produced at vacuum feedthru junctions, these leads pass unsevered through a neoprene rubber pressure seal. Heater leads pass through this same feedthru.

The specimen is placed between the electrodes, and the upper electrode is held firmly in place against the guard electrode with the two springs, A . The guarded electrode may be adjusted by means of three nylon screws, B . The guarded electrode heater and lower thermocouple (C) are insulated from the electrode itself by a film insulator. This insulator can be removed if the lower electrode can be grounded. Adjustments in the lower heater and thermocouple are also made with nylon screws.

Figure 9 depicts the results of a resistance-temperature measurement on cellulose film (American Viscose Division, FMC Corporation, no. 124P-1). Over the entire temperature range from about -30 to +60°C. an exponential behavior is observed. The energy of activation is computed at 0.94 eV. This value is in agreement with earlier measurements (PR1), and is consistent with the results of Lin (<u>11</u>) on dry wood and Murphy (<u>12</u>) on dry paper. It should be recalled from PR1

Figure 8

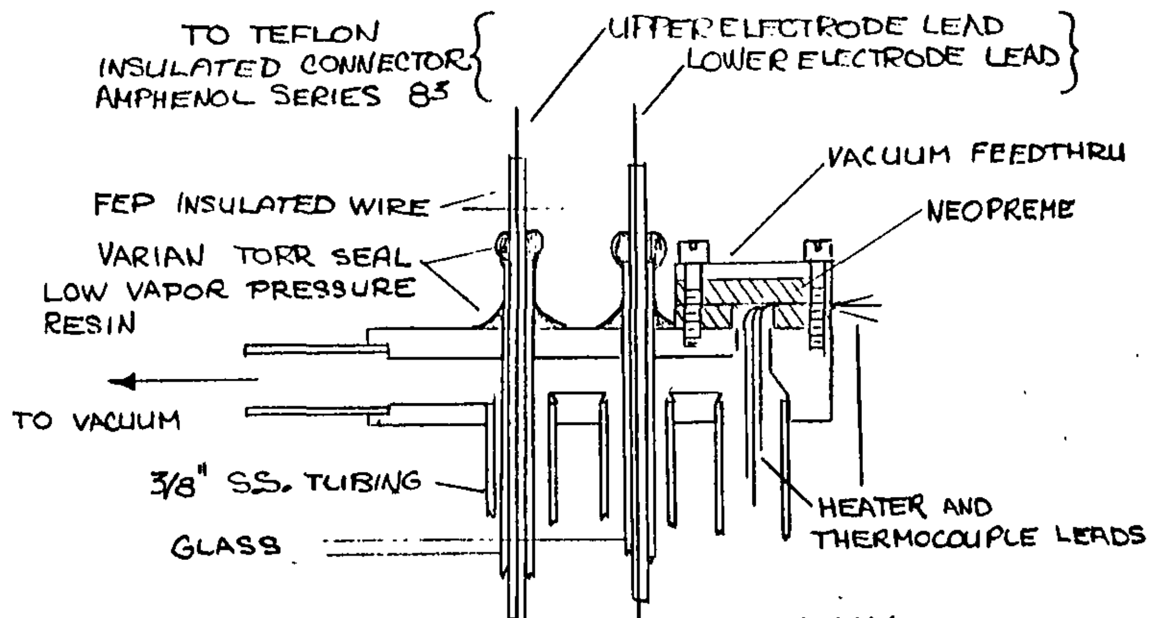

VACUUM FEEDTHRU ASSEMBLY

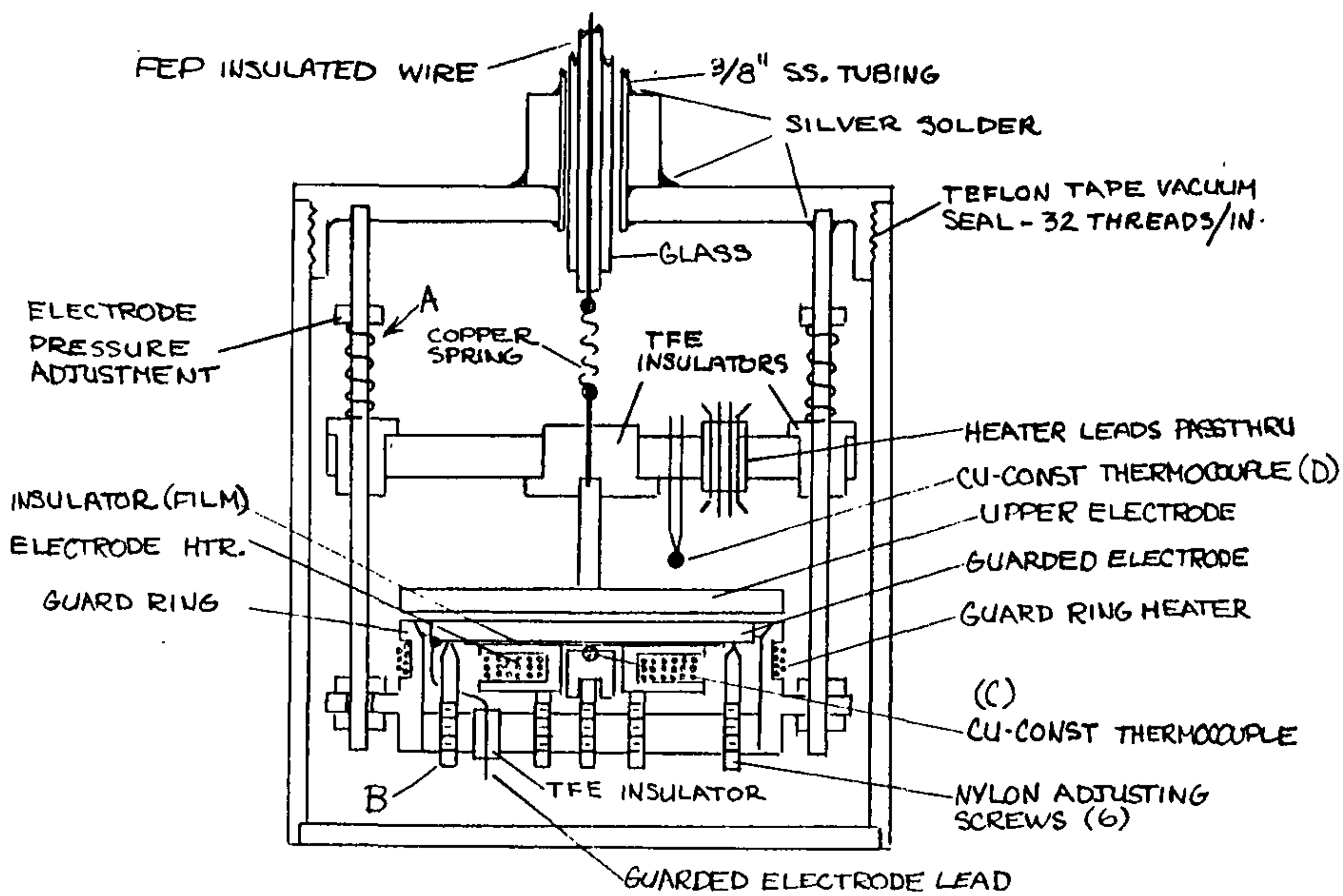

SAMPLE HOLDER

Figure 9

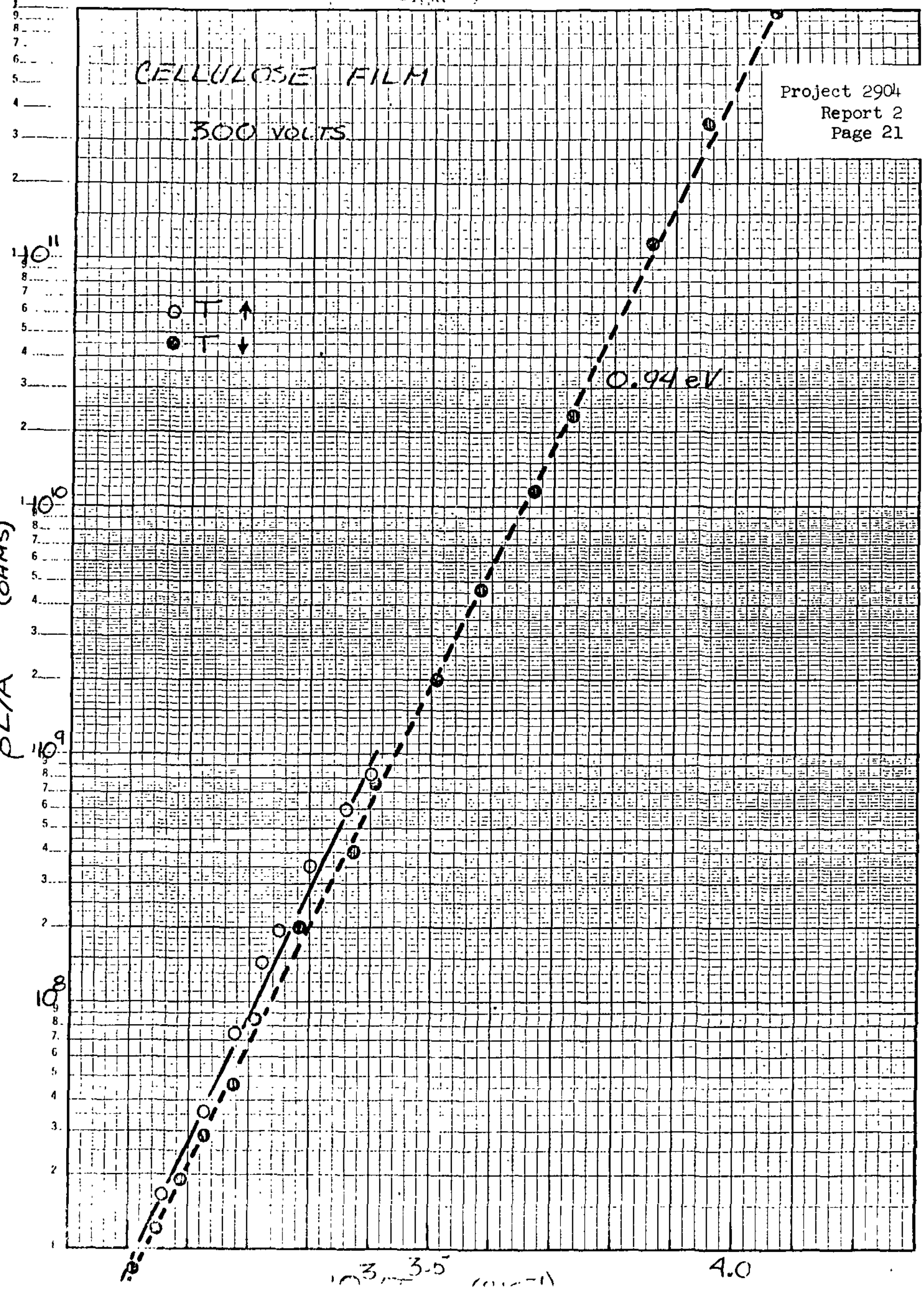
CELLULOSE FILM
300 VOLTS
T ↑
T ↓
0.94 eV
ρL/A (OHMS)
10^11
10^10
10^9
10^8
3.5
4.0

that the magnitude of the applied voltage influences the measured current and thus the resistance. The geometry factor, A/L , has a value of about 5×10^{3} cm. for this specimen and sample holder, and thus the resistivity of the specimen at room temperature is about 1.5×10^{13} ohm·cm.

Figure 10 shows the results of several thermal depolarization measurements. These measurements were made with aluminum electrodes adjacent to the specimen. The location of the maximum, using two different polarization field strengths, occurs at about the same temperature, but the magnitude does not appear to be linear with E_p (if $i_{TD} = 0$ when $E_p = 0$).

At present there are insufficient data to draw conclusions regarding the thermal depolarization effects in cellulose, so the following figures are included mainly for a qualitative discussion. Figure 11 plots the same data as curve 2, Fig. 10. The activation energy is computed as 0.62 eV and τ_o as 2×10^{-9} sec. with $b = 0.03^{\circ}K/sec$. This band is possibly the one shown in Fig. 5, PR1, which had the values $E = 0.67$ eV and $\tau_o = 8 \times 10^{-9}$ sec. with $b = 0.037^{\circ}K/sec$. The difference in the temperatures of the maxima for the two bands may arise from the effects of the plasticizer in the specimens. The specimen of Fig. 11 contains 12.4% glycerine, while for the specimen of Fig. 5, PR1, an attempt had been made to remove some glycerine.

Using the experimental values shown on Fig. 11, the procedure described earlier was used to determine the theoretical curve shown on the figure. The poor agreement at the high temperatures indicates either that the band does not result from orientational polarization or that an additional band is present. Evaluation of the relaxation time, using the graphical integration technique, does reveal two log-linear regions as shown in Fig. 12, thus supporting the latter idea.

Figure 10

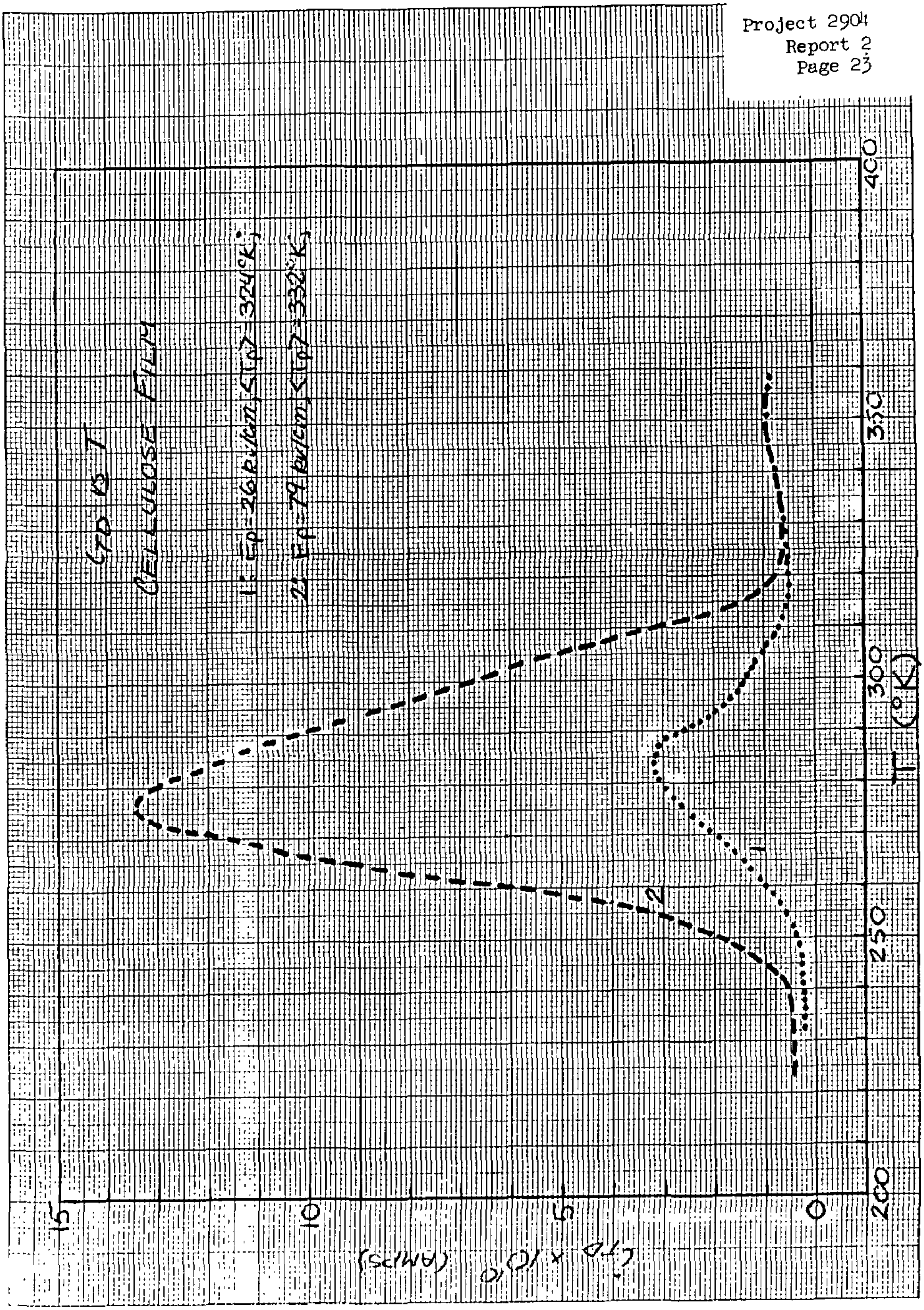
CTD vs T
CELLULOSE FILM
1: Ep-26 kv/cm, ⟨Tp⟩ 324°K
2: Ep-79 kv/cm, ⟨Tp⟩ 332°K
T (°K)
200
250
300
350
400
CTD x 10^10 (AMPS)
0
5
10
15
1
2

Figure 11

Project 2904
Report 2
Page 24

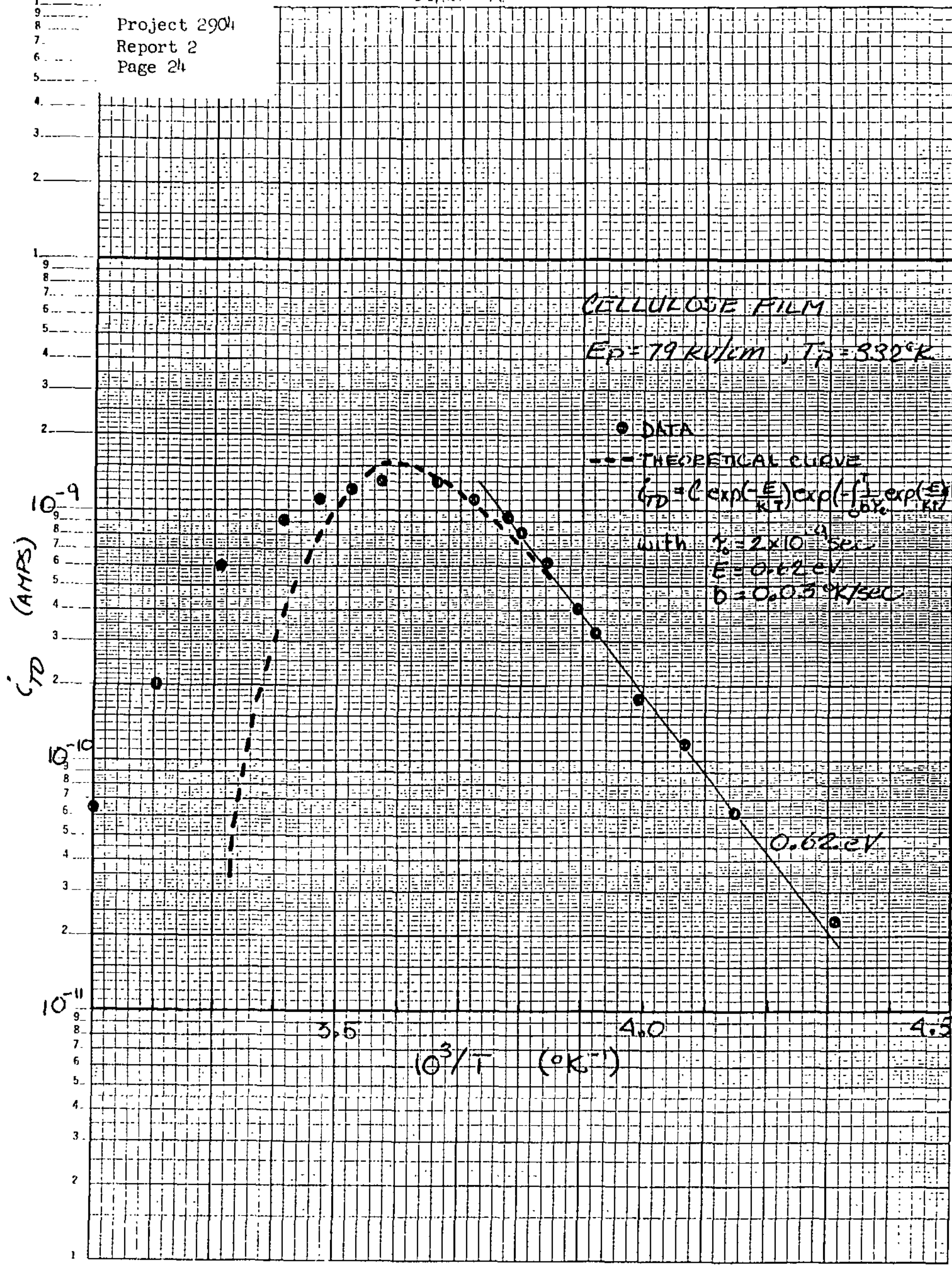

Figure 12

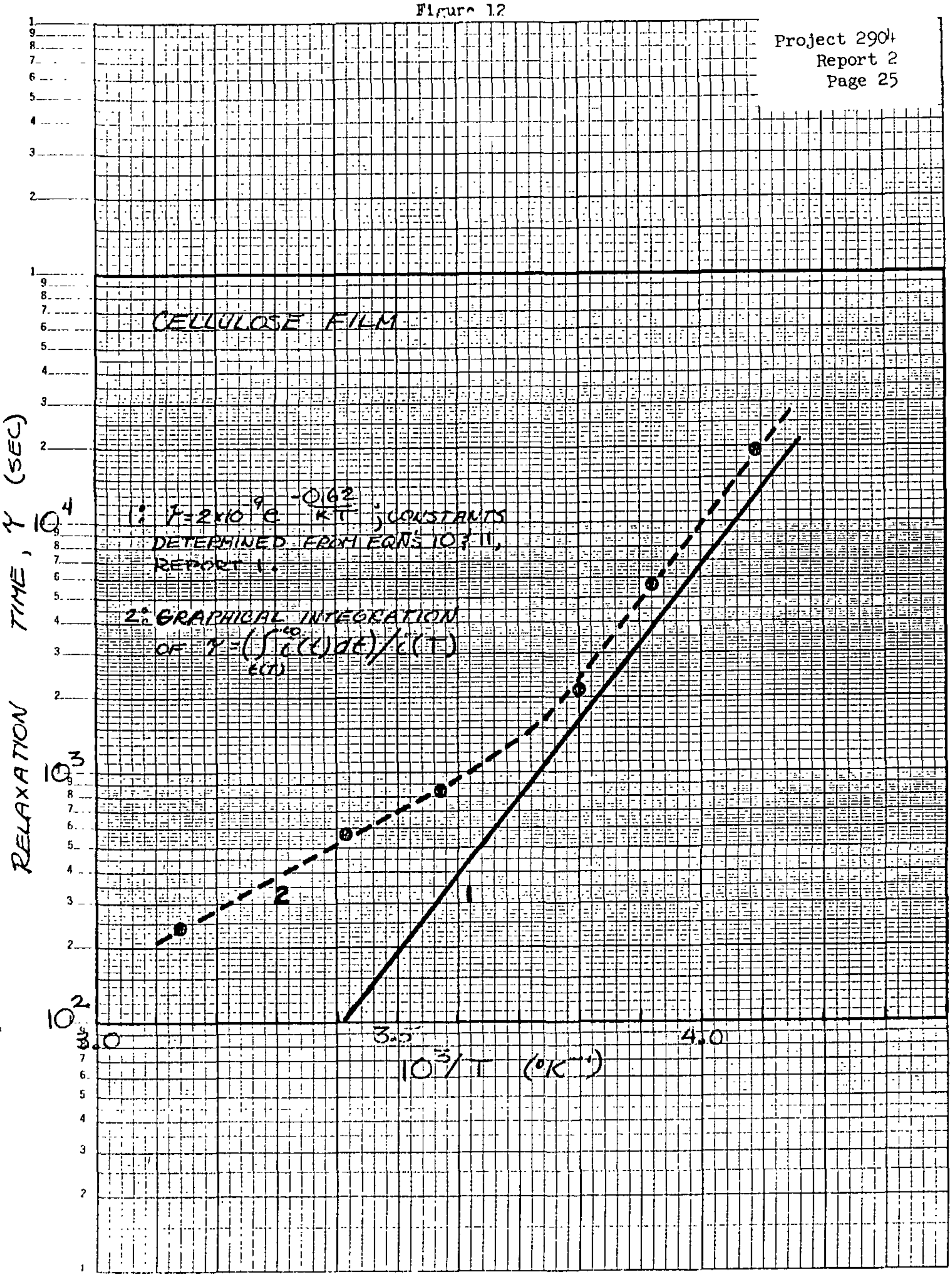
CELLULOSE FILM
1: $\tau = 2\times10^{-9} e^{\frac{-0.62}{KT}}$; CONSTANTS DETERMINED FROM EQNS 10 & 11, REPORT 1.
2: GRAPHICAL INTEGRATION OF $\tau = \left(\int_{t(\tau)}^{\infty} i(t)\,dt\right) / i(\tau)$
RELAXATION TIME, τ (SEC)
10^2
10^3
10^4
3.0
3.5
4.0
$10^3/T$ ($°K^{-1}$)
1
2

Future work will be directed toward acquiring more data in this same temperature range to determine field and polarization temperature dependence, the effects of the plasticizer, and the effects of moisture. In addition, the Mylar results point out the need for studies to distinguish space charge or interfacial polarization bands. This requires measurements using several electrode materials, and thus additionally requires the reproducibility of true orientational polarization bands.

LITERATURE CITED

1. Lilly, A. C., Stweart, L. L., and Henderson, R. M., J. Appl. Physics 41:2007 (1970).
2. Bucci, C., and Fieschi, R., Phys. Review 148:816(1966).
3. Nedetzka, T., Reichle, M., Mayer, A., and Vogel, H., J. Phys. Chem. 74:2652 (1970).
4. Nedetzka, T., Reichle, M., Mayer, A., and Vogel, H., J. Phys. Chem. 74:2659 (1970).
5. Baum, G. A. Project 2904, Report 1. Appleton, Wis., The Institute of Paper Chemistry, Feb. 12, 1970.
6. McCrum, N. G., Read, B. E., and Williams, G. Anelastic and dielectric effects in polymeric solids. New York, J. Wiley and Sons, 1967.
7. Reddish, W., Trans. Faraday Soc. 46:459(1950).
8. Haake, C. H., J. Opt. Soc. Am. 47:649(1957).
9. Amborski, L. E., J. Polymer Sci. 62:331(1962).
10. MacDonald, J. R., J. Chem. Phys. 29:1346(1958); 30:806(1959).
11. Lin, R. T., Forest Products J. 15:506(1965).
12. Murphy, E. J., J. Phys. Chem. Solids 15:66(1960).

APPENDIX I

TIME DEPENDENCE OF POLARIZATION AND CURRENT DENSITY

It is desired to know the polarization and current relaxation, at constant temperature, upon application of an electric field. Assume one type of dipole only and let P and P_s represent the instantaneous and saturated values of the polarization. Also note that the relaxation time, $\tau = \tau_0 \exp(E/kT)$, is a constant if the process is isothermal.

With the application of a field, the rate of increase of polarization is:

$$\frac{dP}{dt} = \frac{+(P_s - P)}{\tau} \qquad (5)\ .$$

Separation of variables, multiplying both sides by -1, and integrating from 0 to t and 0 to P, yields:

$$\int_0^P \frac{-dP}{P_s - P} = \int_0^t \frac{-dt}{\tau}\ ,$$

$$[\ln(P_s - P)]_0^P = [-(t/\tau)]_0^t\ ,$$

or

$$\ln(P_s - P) - \ln P_s = -(t/\tau)\ .$$

Thus, upon solving for P,

$$P = P_s[1 - \exp(-t/\tau)] \qquad (6)\ .$$

The current density, $J = i/A$, where A is the specimen cross-sectional area, is just the time rate of change of polarization, or

$$J = -dP/dt\ .$$

Performing the differentiation upon Equation (6) above, one finds:

$$J = [-P_s/\tau] \exp(-t/\tau) \qquad (7) .$$

APPENDIX II

$i_{TD}(T)$ AND $\tau(T)$ WHEN $R_{ext} \geq R_{sample}$

Consider a polarized specimen connected across an external resistance R. If the specimen is depolarized by heating, and R is much less than the resistance of the specimen, R_x, then $i_{TD}(T) = V(T)/R$. This is the measured current, $i_M(T)$, and it is equal to the actual current, $i_A(T)$ (dropping the subscript TD). If $R_x \leq R$, however, depolarization can occur by a charge migration through the bulk of the specimen itself. In this case, the actual current is the sum of the currents:

$$i_A(T) = V(T)/R + V(T)/R_x = i_M(T) + V(T)/R_x .$$

Rearranging this expression, and noting that $R_x = f(T) = R(T)$, we have the relationship between the actual and measured currents,

$$i_A(T) = i_M(T)[1 + R/R(T)] \qquad (8) .$$

It is also desired to find the relationship between $\tau_A(T)$ and $\tau_M(T)$. In terms of a current-temperature picture, the relaxation time is given by

$$\tau(T) = [b^{-1}\int_T^{\infty} i(T)dT]/i(T) .$$

Using Equation (8) above, the ratio $\tau_A(T)/\tau_M(T)$ is then given by:

$$\tau_A(T)/\tau_M(T) = \frac{\dfrac{\int i_M(T)dT + \int i_M(T)[R/R(T)]dT}{i_M(T) + i_M(T)R/R(T)}}{\int i_M(T)dT/i_M(T)} \; .$$

This simplifies to:

$$\tau_A(T)/\tau_M(T) = \frac{1 + \{\int i_M(T)[R/R(T)]dT/\int i_M(T)dT\}}{1 + [R/R(T)]} \qquad (9) \; .$$

The numerator can be evaluated by plotting $i_M(T)R/R(T)$ as a function of T and then graphically evaluating the integral.